FRONTIERS OF PHYSICS

TOPICAL REVIEW
Volume 18 / Issue 2 / 21304 / 2023

Intrinsic magnetic topological materials

Yuan Wang*, Fayuan Zhang*, Meng Zeng*, Hongyi Sun*, Zhanyang Hao, Yongqing Cai, Hongtao Rong, Chengcheng Zhang, Cai Liu, Xiaoming Ma, Le Wang, Shu Guo, Junhao Lin, Qihang Liu, Chang Liu†, Chaoyu Chen‡

Shenzhen Institute for Quantum Science and Engineering (SIQSE) and Department of Physics, Southern University of Science and Technology (SUSTech), Shenzhen 518055, China
Corresponding authors. E-mail: †liuc@sustech.edu.cn, ‡chency@sustech.edu.cn
*These authors contributed equally to the work.
Received December 18, 2022; accepted January 6, 2023

ABSTRACT

Topological states of matter possess bulk electronic structures categorized by topological invariants and edge/surface states due to the bulk-boundary correspondence. Topological materials hold great potential in the development of dissipationless spintronics, information storage and quantum computation, particularly if combined with magnetic order intrinsically or extrinsically. Here, we review the recent progress in the exploration of intrinsic magnetic topological materials, including but not limited to magnetic topological insulators, magnetic topological metals, and magnetic Weyl semimetals. We pay special attention to their characteristic band features such as the gap of topological surface state, gapped Dirac cone induced by magnetization (either bulk or surface), Weyl nodal point/line and Fermi arc, as well as the exotic transport responses resulting from such band features. We conclude with a brief envision for experimental explorations of new physics or effects by incorporating other orders in intrinsic magnetic topological materials.

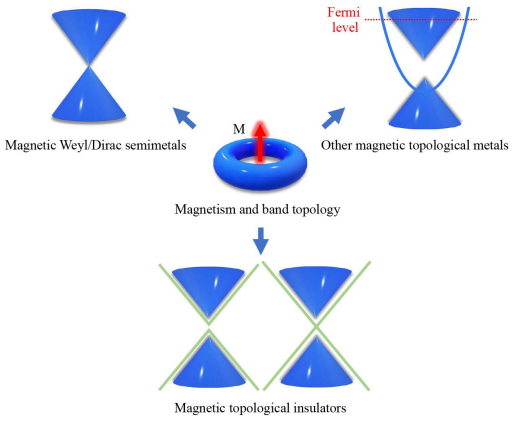

Keywords intrinsic magnetic topological insulator, magnetic topological metals, magnetic Weyl semimetal, topological surface states, magnetic gap

Contents

*Special Topic: Embracing the Quantum Era: Celebrating the 5th Anniversary of Shenzhen Institute for Quantum Science and Engineering (Eds.: Dapeng Yu, Dawei Lu & Zhimin Liao).

Higher Education Press

https://doi.org/10.1007/s11467-022-1250-6

1 Introduction

The first two decades of the new millennium have witnessed the surge of topological states of matter, whose electronic structures can be categorized by topological invariants. The prediction [1–6] and realization [7–11] of two-dimensional (2D) and three-dimensional (3D) topological insulators (TIs) have caused a paradigm shift to predict, understand and make use of quantum materials based on the topology of their band structures. Started with the 2D TI, quantum spin Hall (QSH) effect realized based on HgTe/CdTe quantum well [6, 7] has revealed to the world the fundamental novelty and potential application of topological materials. QSH state is insulating in the bulk but has a pair of one-dimensional (1D) conducting edge states protected by time-reversal symmetry. Electrons in the 1D edge states move without elastic backscattering by nonmagnetic impurities, holding potential for dissipationless spintronics. Likely, a 3D strong TI is also insulating in the bulk and has 2D gapless topological surface states (TSSs). 3D TI was first realized based on Bi–Sb alloys [8] and then on Bi_2Se_3 family [5, 9–11]. The robustness of topological protection to the TSSs from nonmagnetic perturbations has been experimentally demonstrated [12–14], pointing to feasible electronic and spintronic applications. Importantly, based on magnetically doped Bi_2Te_3 films, quantum anomalous Hall (QAH) effect was realized [15, 16], a milestone towards low-power-consumption electronics without the need for applied magnetic field.

Besides insulators, quantum materials can also be metals and semimetals according to the detailed band structure around the Fermi level. After TIs, topological semimetals emerged as novel states of matter with degenerate band crossing close to which the band dispersion can be described by the massless 3D Weyl and Dirac equations [17–23]. In a Dirac semimetal (DSM), the conduction and valence bands touch at discrete (Dirac) points with linear dispersion, forming bulk (3D) Dirac fermions. Given broken time-reversal or inversion symmetry, 3D Dirac fermion can be separated in the momentum space into two Weyl fermions (chiral massless fermions as a description of neutrinos with neglected mass in high-energy physics), resulting into topological Weyl semimetals (WSMs). Such nontrivial electronic features could bring into novel electrical and thermal transport behaviors such as anomalous Hall effect (AHE), anomalous Nernst effect, chiral anomaly signified by negative magnetoresistance and non-saturating magnetoresistance (see Refs. [17, 24–26] for comprehensive reviews). Such properties come from the enhanced Berry curvature hosted in the Dirac/Weyl type band structure, which exhibits extreme responses to external stimuli such as magnetic field, voltage or current bias, temperature gradient and optical excitation.

There have been hundreds of materials predicted as 3D strong TI [27–29] and dozens of them have been experimentally verified, usually through direct observation of their TSS Dirac cones by angle-resolved photoemission spectroscopy (ARPES) [30–32]. By comparison, magnetic TIs, especially intrinsic magnetic TIs, are limited in the material candidates. So far there is only $(MnBi_2Te_4)\cdot(Bi_2Te_3)_n$ $(n = 0, 1, 2, 3)$ family which has been intensively studied as an intrinsic magnetic TI [33–39]. There are also many materials predicted and demonstrated as DSMs and WSMs, most of which are time-reversal invariant and only few materials have been studied as magnetic WSMs [17, 24–26]. Recently, there appeared several layered material families with hexagonal/Kagome lattices which host Dirac cones gapped by ferromagnetic (FM)/antiferromagnetic (AFM) order, such as Fe_3Sn_2 family [40]. In the 2D limit, these systems with gapped Dirac cones can be viewed as Chern insulating phase with quantized anomalous Hall conductance [41], given the Fermi level is positioned in the Dirac gap. In this sense, these materials share the same topological characters (the Chern number C) as intrinsic magnetic TIs. However, for 3D materials, the band structure is complicated by the coexisting trivial bands which locate at the same energy region as the Dirac gap, rendering such materials in metal phase with coexisting trivial and nontrivial conduction. Consequently, we feel it more appropriate to term such materials as magnetic topological metals. While quantized transport response from the edge conduction can be realized in intrinsic magnetic TIs by tuning the Fermi level in the gap of both bulk and surface bands, there is always transport contribution from the trivial bands in magnetic topological metals no matter where the Fermi level is. It is noted that there is no strict theoretical picture describing topological metals since the metallicity does not come from band topology but trivial bands. We choose this term only to emphasize its distinction from intrinsic magnetic TIs and topological SMs.

In this review, we focus on the recent progress in the exploration of these various kinds of intrinsic magnetic topological materials, categorized mainly into three groups: intrinsic magnetic (TIs), magnetic Weyl/Dirac semimetals and other magnetic topological metals. We will present representative materials for these novel topological states of matter, pay special attention to their characteristic band features such as the gap of topological surface state Dirac cone, gapped bulk Dirac cone, Weyl nodal point/line and Fermi arc, as well as the exotic transport responses resulting from such band features. There are also other intrinsic magnetic topological states of matter which have been proposed theoretically, yet lacking affirmative experimental evidence, such as

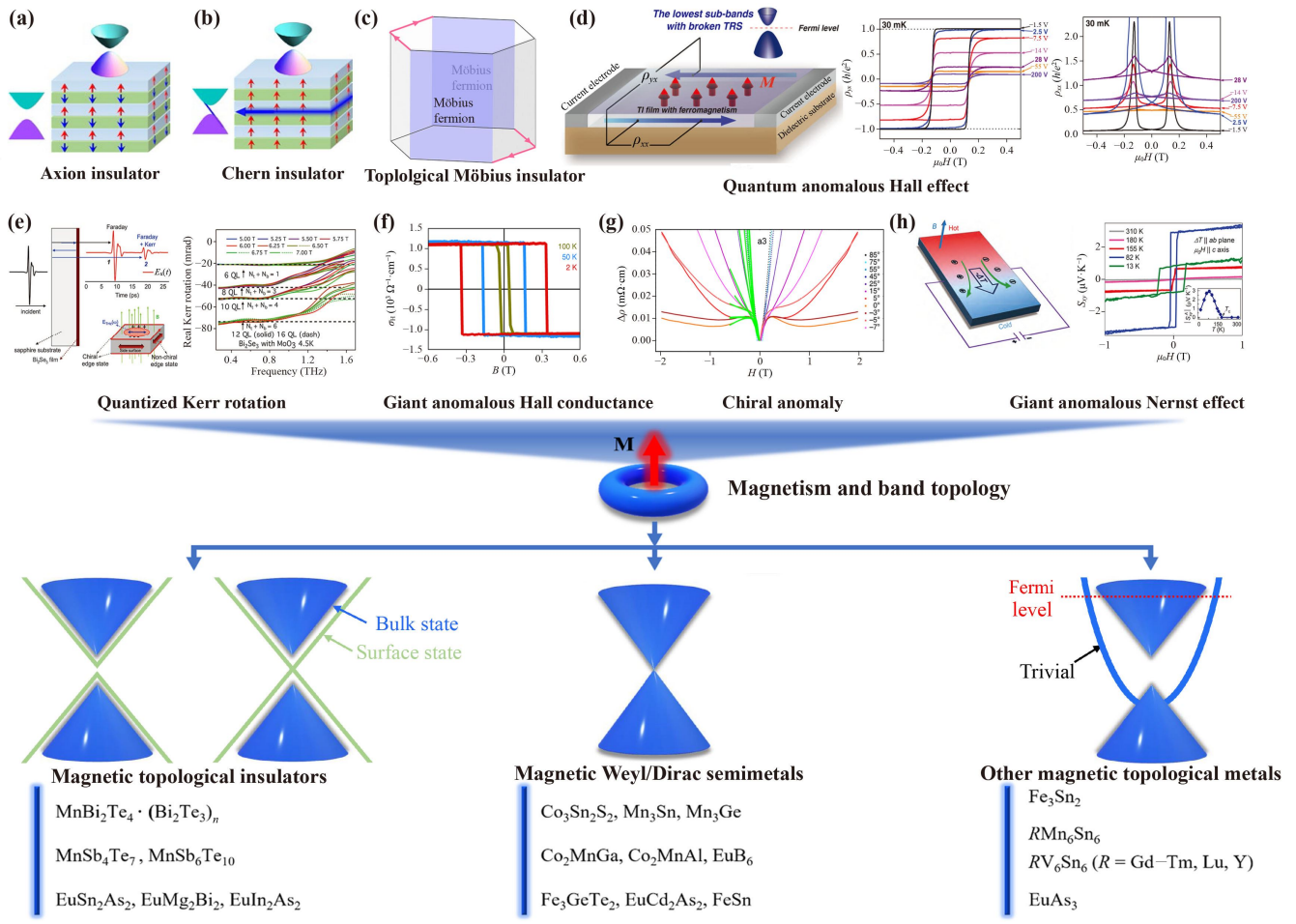

Fig. 1 Family tree of intrinsic magnetic topological materials. The combination of intrinsic magnetism and band topology gives birth to exotic states of matter such as axion insulator (**a**, reproduced from Ref. [45]), Chern insulator (**b**, reproduced from Ref. [45]), and topological Möbius insulator (**c**, reproduced from Ref. [44]), manifesting novel properties such as QAH effect (**d**, reproduced from Ref. [46]), quantized magneto–optical effect (Kerr rotation, **e**, reproduced from Ref. [47]), giant anomalous Hall conductance (**f**, reproduced from Ref. [48]), chiral anomaly (**g**, reproduced from Ref. [49]), and giant anomalous Nernst effect (**h**, reproduced from Refs. [50, 51]). Magnetic topological materials can be roughly categorized into magnetic TIs, magnetic Weyl/Dirac semimetals and other magnetic topological metals, with each of these states being realized based on various materials systems as listed. As schematically shown by the band cartoon, magnetic TIs are characterized by gapped bulk state and TSSs which can be either gapped or gapless, depending on the specific magnetic structure and surface termination; magnetic Weyl/Dirac semimetals are characterized by gapless band crossings which can be described by Weyl/Dirac equation; other magnetic topological metals share gapped bulk state and TSSs similar to the magnetic TIs, but compromised by the coexisting trivial bands.

topological Möbius insulators [42–44]. We briefly discuss the opportunities to explore new states of matter and novel physical properties based on intrinsic magnetic topological materials.

2 Intrinsic magnetic topological insulator

Intrinsic magnetic TIs provide an excellent platform for the study of exotic quantum states, such as QAH states, chiral Majorana fermions, and axion states [33–39], arising from the interplay between band topology and magnetism. Among them, QAH effect is of fundamental importance in the field of spintronics due to its non-dissipative properties in transport. One approach to realize it is to find a 2D TI that comprises long-range magnetic order. Introducing magnetism into the 2D TI can break the time-reversal symmetry, such that one direction of spin channels will be canceled. Although QAH effect has been proposed theoretically in the last century [41], it is until 2013 when quantized edge resistance (h/e^2) was experimentally observed on Cr-doped (Bi, Sb)$_2$Te$_3$ thin films [15]. The chemical doping results into inhomogeneity in the band structure (gap, carrier density) and consequently extremely low quantization temperature. Therefore, intrinsic magnetic states of

matter with uniform long-range magnetic order are highly desired.

As first discussed in the theoretical proposal of AFM TIs in 2010 [52], both time-reversal symmetry Θ and fractional translation $T_{1/2}$ are broken but the combination $S = \Theta T_{1/2}$ is preserved in AFM TI, leading to a topologically nontrivial phase which shares with 3D strong TI similar topological Z_2 invariant and quantized magnetoelectric effect. The material realization of an intrinsic AFM TI was not initiated until 2017. "Magnetic extension" picture proposed that by inserting MnTe bilayer into the quintuple layer of Bi_2Te_3, the system tends to form septuple layers of $MnBi_2Te_4$, hosting a robust QAH state [53, 54]. The material was first experimentally realized by molecular beam epitaxy (MBE) [55]. Subsequent theoretical works revealed its colorful physics and properties [56–59]. Since the successful preparation of single crystal $MnBi_2Te_4$, the surge of intrinsic magnetic TIs based on $MnBi_2Te_4$ family started. Following the discovery of $MnBi_2Te_4$, a series of superlattices of this family were discovered, denoted as $MnBi_2Te_4{\cdot}(Bi_2Te_3)_n$ (n = 1, 2, 3) [60–62]. In addition, we will briefly introduce other intrinsic magnetic TI candidates such as $MnSb_2Te_4{\cdot}(Bi_2Te_3)_n$ (n = 1, 2) and $EuSn_2As_2$ families.

2.1 $MnBi_2Te_4{\cdot}(Bi_2Te_3)_n$

In 2013, Lee *et al.* [63] synthesized the polycrystalline powder of $MnBi_2Te_4$ by the flux-method. In 2017, from MBE growth of heterostructure composed of MnSe and Bi_2Se_3, it was found that the topological surface state of this structure is located on the surface of the whole system, rather than at the interface of the two materials like other topological heterostructures. It was realized that the layered structure of MnSe and Bi_2Se_3 is a new type of single crystal, $MnBi_2Se_4$. Such transformation is also applicable to $MnBi_2Te_4$ [53, 54, 64, 65], and it is $MnBi_2Te_4$ which is the focus of intrinsic magnetic TI study due to its desirable magnetic, electronic, and structural properties.

The structure of $MnBi_2Te_4$ was refined to be in the hexagonal space group $R\bar{3}m$ (No. 166) [60]. Its minimum structural unit is composed of seven atomic layers with stacking order Te–Bi–Te–Mn–Te–Bi–Te, which is called a septuple-layer (SL) and the adjacent layers are bonded by van der Waals force, as shown in Fig. 2(a). The unit cell of $MnBi_2Te_4$ is composed of three SLs stacked in the –A–B–C– fashion, and its lattice constant c is about 4.07 nm. Its Neel temperature T_N (124) $\approx$ 24.4 K [66], above which the AFM order is transformed into paramagnetic (PM) order [Fig. 2(b)]. Neutron diffraction experiments point out that the ground state magnetic structure of $MnBi_2Te_4$ is the A-type AFM phase [66, 67]. The magnetic moment of each SL points out of plane, and the magnetic moments of adjacent layers are opposite. Of course, if Bi_2Te_3 quintuple-layers (QLs) is inserted between SLs, we can get $MnBi_4Te_7$, $MnBi_6Te_{10}$, and $MnBi_8Te_{13}$ superlattices [60–62, 68]. $MnBi_4Te_7$ can

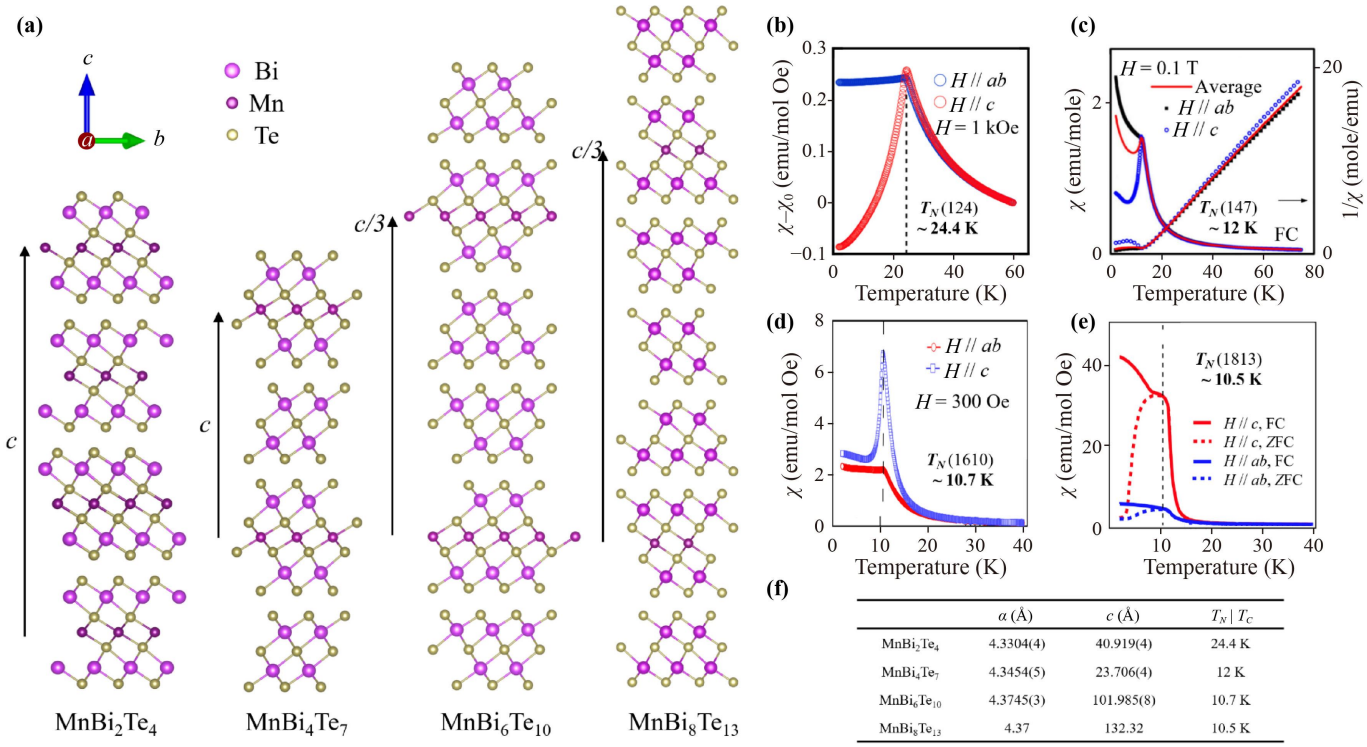

	a (Å)	c (Å)	T_N | T_c
$MnBi_2Te_4$	4.3304(4)	40.919(4)	24.4 K
$MnBi_4Te_7$	4.3454(5)	23.706(4)	12 K
$MnBi_6Te_{10}$	4.3745(3)	101.985(8)	10.7 K
$MnBi_8Te_{13}$	4.37	132.32	10.5 K

Fig. 2 **(a)** Crystal structure of $MnBi_2Te_4{\cdot}(Bi_2Te_3)_n$. **(b–e)** Magnetic properties of $MnBi_2Te_4{\cdot}(Bi_2Te_3)_n$ (n = 0, 1, 2, 3) [69–72]. **(f)** Summary of lattice constants for $MnBi_2Te_4{\cdot}(Bi_2Te_3)_n$.

be regarded as a sandwich structure formed by inserting one QL into each SL. Similarly, $MnBi_6Te_{10}$ and $MnBi_8Te_{13}$ are formed by inserting two or three QLs in each SL respectively. Note that the space group of $MnBi_2Te_4$, $MnBi_6Te_{10}$, and $MnBi_8Te_{13}$ is $R\bar{3}m$, but the space group of $MnBi_4Te_7$ is $P\bar{3}m1$. Since the distance between two SLs in $MnBi_4Te_7$ and $MnBi_6Te_{10}$ is larger than that in $MnBi_2Te_4$, their interlayer AFM coupling is weaker. The results of magnetic transport measurement show that the AFM-PM transition temperature of $MnBi_4Te_7$ is $T_N \approx 12$ K [Fig. 2(c)] and that of $MnBi_6Te_{10}$ is $T_N \approx 10.7$ K [Fig. 2(d)]. More interestingly, with further increasing SL spacing, the compound of $MnBi_8Te_{13}$ has become the first intrinsic FM TI with $T_C \approx 10.5$ K [Fig. 2(e)]. The lattice constants and magnetic transition temperatures of these different compounds are also summarized in Fig. 2(f).

The band structure of $MnBi_2Te_4$, as the first intrinsic magnetic TI, has been intensively studied [59, 69, 73–76] and the TSS inside the bulk gap is the focus of attention. At the early stage, a sizable gap was found for the TSS Dirac cone with temperature-independent behavior [59, 77, 78]. However, subsequent ARPES works with systematic photon-energy-dependent measurement and higher energy and momentum resolution have revealed the nearly gapless behavior of TSS [69, 73–76, 79–83], showing sample and location dependence [Fig. 3(a)]. Here we use the term "nearly gapless" to describe the experimental observation that the size of Dirac gap varying from being vanishing to dozens of millielectronvolts, being much smaller than expected by theoretical calculation [56–59]. Such behaviors suggest much reduced effective magnetic moments felt by the TSS, which may arise from surface magnetic reconstruction or TSS redistribution (extension to the bulk). Currently there are several proposed mechanisms which may lead to one of these two phenomena yet none of them has been experimentally validated. Please refer to our recent review for more details [33].

Since the SLs and QLs in the heterostructure members of this family ($MnBi_4Te_7$, $MnBi_6Te_{10}$, $MnBi_8Te_{13}$) are combined by van der Waals forces, there are different terminations after cleaving the sample. As shown in Figs. 3(b–d), the band structure on SL-termination is very similar to that of $MnBi_2Te_4$, and the band structure on QL- and double QL-terminations show

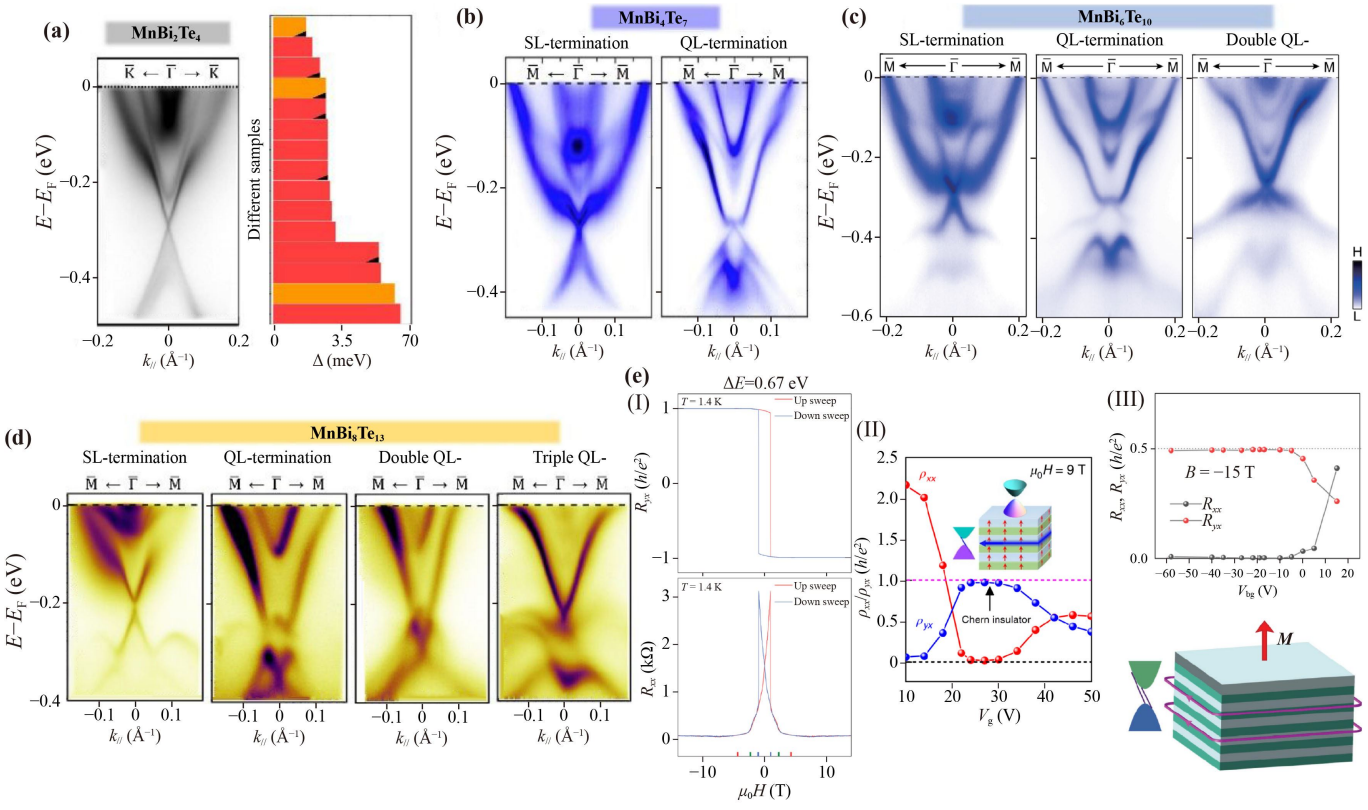

Fig. 3 **(a)** Observation of nearly gapless TSS in $MnBi_2Te_4$ single crystal (0001) surface (left, reproduced from Ref. [69]) and the variation of TSS gap in different samples (right, reproduced from Ref. [83]). **(b, c, d)** APRES spectra measured from the SL- and QL- (double QL-, triple QL-) terminations of $MnBi_4Te_7$ [97], $MnBi_6Te_{10}$ [79] and $MnBi_8Te_{13}$ [72], respectively. **(e)** Observation of QAH effect (I, reproduced from Ref. [93]), axion insulator phase (II, reproduced from Ref. [45]) and high-Chern number Chern insulator (III, reproduced from Ref. [94]) based on $MnBi_2Te_4$ films with different number of layers.

hybridization features between the TSS and certain bulk bands [70, 71, 79, 84–92]. Again, no signature of sizable magnetic gap can be found for the TSS from all the different terminations of AFM members. The sizable magnetic gap of TSS was realized based on the SL-termination of FM $MnBi_8Te_{13}$, with the gap size decreasing monotonically with increasing temperature and closing right at the Curie temperature [72].

Although the lack of sizable magnetic gap of TSS obscures the realization of topological quantized transport at high temperature (say, at the level of AFM transition temperature), QAH effect has indeed been realized at low temperature [1.4 K, Fig. 3(e)] based on 5 QLs films of $MnBi_2Te_4$, key evidence of a 2D Chern insulator [93]. The characteristics of an axion insulator state were also observed at zero magnetic field based on 6 SLs [45]. Under a perpendicular magnetic field (15 T), characteristics of high-Chern-number quantum Hall effect without Landau levels and contributed by dissipationless chiral edge states are observed, indicating a high Chern number Chern insulator with $C = 2$ (9, 10 SLs) [94]. The *A*-type AFM configuration exhibits layer Hall effect in which electrons from the top and bottom layers deflect in opposite directions due to the layer-locked Berry curvature, resulting in the characteristic of the axion insulator state (6 SLs) [95, 96]. We envision that half quantized Hall transport at the level of 10 K can be realized based on the SL-termination of FM $MnBi_8Te_{13}$ with sizable magnetic TSS gap [72].

2.2 $MnSb_2Te_4{\cdot}(Sb_2Te_3)_n$

Since the successful synthesis of $MnBi_2Te_4{\cdot}(Bi_2Te_3)_n$ single crystals, elemental substitutions have been explored in order to manipulate its magnetic and electronic properties. It turns out the Bi site can be completely substituted by Sb atoms. The resulting $MnSb_2Te_4{\cdot}(Sb_2Te_3)_n$ family of materials are currently under intensive investigation. Theoretically, this family ($n = 0, 1, 2$) is also predicted to host similar AFM ground state and AFM TI phase [98, 99], yet there lacks consistency between/among experiments and calculations on the exact magnetic ground state and band topology of $MnSb_2Te_4$ [100–106]. Notably, ARPES results reveal significant hole doping for all the members studied so far, leaving the detailed TSS Dirac cone structure not straightforward to study [105, 107].

The crystal structure of $MnSb_4Te_7$ adapts a space group of $P\bar{3}m1$. The Mn layer constitutes a long-range magnetic order with moments along the *c* direction [Figs. 4(a, b)] [107] (*A*-type AFM with $T_N = 13.5$ K). ARPES measurement also reveals hole doping for the band structure with expected Dirac cone located at 180 meV above the Fermi level [Fig. 4(c)]. Pressure experiments and DFT calculations have revealed multiple topological phases corresponding to various magnetic structures and the emergence of superconductivity [Fig. 4(d)] [98, 106–110]. Similar hole doping and multiple magnetic topological phases have also been found in $MnSb_6Te_{10}$,

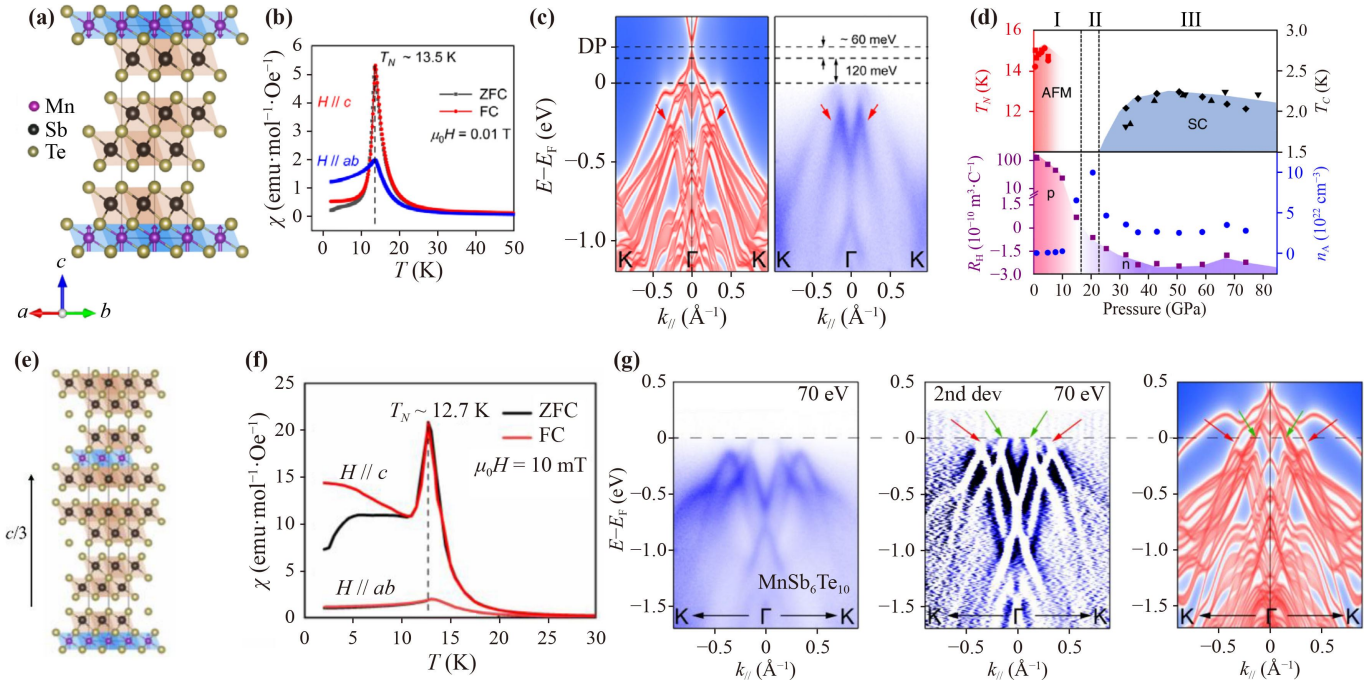

Fig. 4 Crystal structure **(a, e)**, magnetic transport properties **(b, f)** and band structure **(c, g)** of $MnSb_4Te_7$ and $MnSb_6Te_{10}$, respectively [107,111]. **(d)** The pressure dependence of superconducting transition temperature T_C, AFM transition temperature T_N (upper panel), Hall coefficient R_H and carrier concentration (lower panel) at 10 K (different symbols represent different samples in the upper panel) [110].

an FM member of this family at its ground state [Figs. 4(f, g)] [111]. Considering the universal electron doping behavior in $MnBi_2Te_4\cdot(Bi_2Te_3)_n$ family, it is natural to expect carrier tunability and magnetic manipulation based on the mutual substitution of Sb and Bi in $Mn(Bi, Sb)_2Te_4\cdot((Bi, Sb)_2Te_3)_n$ series. In fact, a tunable TSS Dirac gap varying from being gapless to larger than 100 meV has been reported in Sb doped $MnBi_2Te_4$, with its gap size proportional to the doping level [112].

Except $MnBi_2Te_4\cdot(Bi_2Te_3)_n$ and $MnSb_2Te_4\cdot(Sb_2Te_3)_n$ families, it is noted that $MnBi_2Se_4$ in the $R\bar{3}m$ space group shares the same magnetic and topological properties of $MnBi_2Te_4$. This phase turns out to be unstable in the bulk crystal form. Recent efforts have succeeded in synthesizing ultrathin films of $MnBi_2Se_4$ using nonequilibrium MBE [113]. Its magnetic structure, however, deviates from the expected A-type AFMz structure and the response of TSS Dirac cone to the magnetic order remains to be investigated.

2.3 EuM_2X_2 (M = metal; and X = Group 14 or 15 element)

$EuSn_2As_2$ belongs to the group of compounds with formula AM_2X_2 (A = alkali, alkaline earth, or rare earth cation; M = metal; and X = Group 14 or 15 element). Here we focus on the A = Eu compounds with intrinsic AFM order. The M site can be occupied by various types of metals such as Mg, In and Sn. $EuSn_2As_2$, as an important member in intrinsic magnetic TI family, crystallizes in the hexagonal space group $R\bar{3}m$. The Eu atoms are triangularly distributed and sandwiched by two honeycomb SnAs layers to form a layered structure [Fig. 5(a)]. The magnetic moment provided by Eu atom forms an A-type AFM configuration with $T_N = 25$ K [74, 114] [Fig. 5(b)]. ARPES measurements have revealed a TSS Dirac cone locating ~ 0.4 eV above the Fermi level at the PM phase, suggesting a strong 3D TI phase [Fig. 5(c)]. Yet no observable change of the TSS or carrier concentration can be found in the AFM state, indicating weak coupling between the Eu moments and low-energy bands [74, 121]. Magnetic property and transport measurements report negative magnetoresistance and complicated magnetic transitions from an AFM state to a canted ferromagnetic state and then to a polarized FM state as the magnetic field increases [121, 122]. Electrical resistance measurements under pressure reveal an insulator-metal-superconductor transition at low temperature around 5 and 15 GPa [Fig. 5(d)]. A new $C2/m$ phase appears when the pressure is higher than 14 GPa. As the pressure continues to increase, the superconductivity persists up to 30.8 GPa with T_C maintaining a constant value ~ 4 K [119]. It is also found that the pressure has an enhancement effect on the AFM transition temperature and negative magnetoresistance [123].

For $EuMg_2Bi_2$, it crystallizes into the tetragonal $CaAl_2Si_2$ structure type with space group $P\bar{3}m1$ (No. 164) [117] [Fig. 5(e)]. Magnetic property measurements revealed AFM transition temperature $T_N \sim 7$ K with slight anisotropy and positive Curie-Weiss temperature indicating FM interaction between Eu atoms ($7.8\ \mu_B$) [Fig. 5(f)]. Like Mn–Bi–Te family, AFM configuration between FM layers of Eu is established. The difference is that the moments point out-of-plane in Mn–Bi–Te but in-plane for $EuMg_2Bi_2$. ARPES measurements and DFT calculations have revealed Dirac surface state features and nontrivial band topology [Figs. 5(g, h)], suggesting $EuMg_2Bi_2$ as a magnetic topological insulator candidate

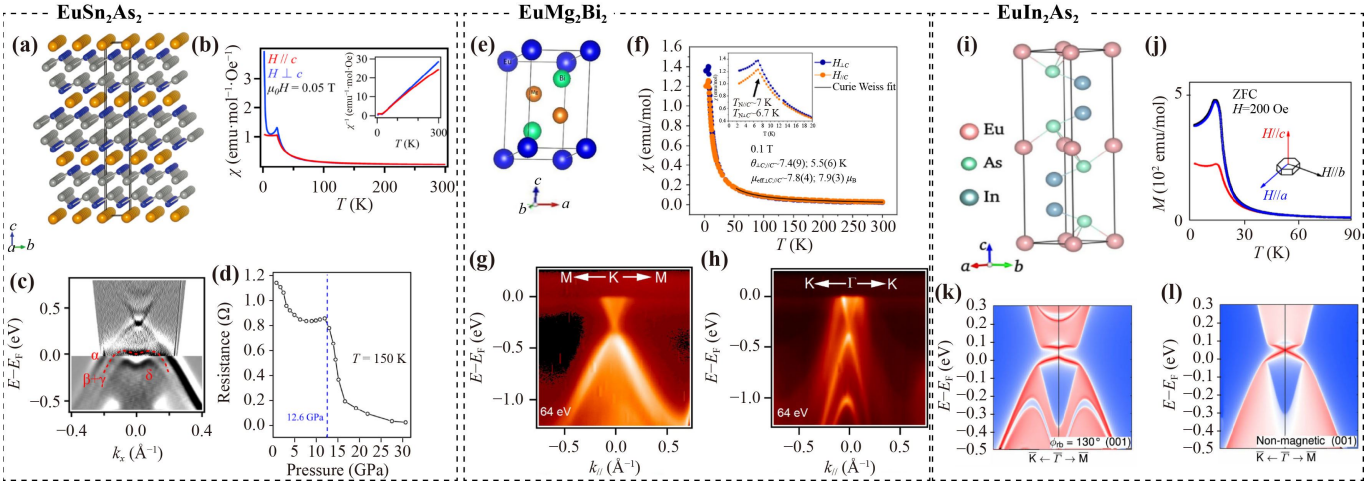

Fig. 5 **(a, e, i)** Crystal structures of $EuSn_2As_2$ [114], $EuMg_2Bi_2$ [115] and $EuIn_2As_2$ [116], respectively. In (a), Eu atoms are shown in orange, Sn in gray and As in bule. **(b, f, j)** Magnetic transport properties of $EuSn_2As_2$ [74], $EuMg_2Bi_2$ [117] and $EuIn_2As_2$ [118], respectively. **(c)** Band structure of $EuSn_2As_2$ measured by pump-probe ARPES [74]. **(d)** The pressure dependence of resistance for $EuSn_2As_2$ [119]. **(g, h)** Band structure of $EuMg_2Bi_2$ along M–K–M and K–Γ–K, respectively [115]. **(k, l)** Calculated band structure of $EuIn_2As_2$ [120].

[115, 117].

$EuIn_2As_2$ crystallizes into the hexagonal space group $P6_3/mmc$, containing layers of Eu^{2+} cations separated by $In_2As_2^{2-}$ layers along the crystallographic c-axis [124] [Fig. 5(i)]. Magnetic property and neutron diffraction measurements have determined a colinear AFM ground state with the moments lying in the ab-plane [118, 120, 124, 125] [Fig. 5(j)]. Furthermore, a complicated broken helix order is reported by neutron diffraction, tripling the unit cell along c-axis. $EuIn_2As_2$ was predicted as a high-order topological axion insulator candidate [120, 126] protected by the magnetic crystalline symmetry. Such a state has gapless TSS Dirac cone at the symmetry-protected termination and gapped ones at other surfaces [Figs. 5(k–l)]. However, like other AM_2X_2 compounds, its hole-doping nature as observed by ARPES [116, 118] and scanning tunneling microscope (STM) [127] has prevented the detailed study on the TSS band structure, especially the gap behavior. Further chemical and band structure engineering are strongly called for to tune the chemical potential for access to the TSS Dirac point in this family.

There are also theoretical calculations which predict materials such as several $Eu_5M_2X_6$ (M = metal, X = pnictide) Zintl compounds [128, 129], 2D $EuCd_2Bi_2$ [130], and $NiTl_2S_4$ [131] to be intrinsic magnetic TI candidates yet their growth, band structure, magnetic structure and band topology remain to be investigated.

3 Magnetic Weyl/Dirac semimetals

In a DSM, two doubly degenerate bands contact at discrete momentum points called Dirac points and disperse linearly along all directions around these points. The four-fold degenerate Dirac points need symmetries to ensure their existence, such as time-reversal symmetry T, inversion symmetry P, rotational symmetry and nonsymmorphic symmetry. In a DSM with TP symmetry, when either T or P is broken, each doubly degenerate band is lifted, so that the Dirac cones can split into multiple Weyl cones, giving birth to WSMs. However, in 3D systems with AFM order that breaks both T and P but respect their combination PT, four-fold degenerate Dirac points can still exist, resulting into AFM DSM [132]. Such consideration has also been generalized to 2D systems [133–135].

In magnetic WSMs, spin-polarized conduction and valence bands touch at finite number of nodes, forming pairs of Weyl nodes. In each pair, the quasiparticles carry opposite chirality and can be viewed as the "source" ("+" chirality) and the "sink" ("–" chirality) of the Berry curvature. Odd pairs of Weyl nodes with opposite chirality can be expected in systems with T symmetry breaking, such as $Co_3Sn_2S_2$ [136, 137] and Mn_3X (X = Sn, Ge) [138–140]; while for systems with time-reversal symmetry T, the total number of Weyl nodes pairs must be even. Noncentrosymmetric WSMs belong to this category, such as TaAs family [141–144]. If P and T symmetries are both preserved, Weyl nodes with opposite chirality can merge at the same momentum and form a four-fold Dirac point (assisted by additional crystal symmetry), such as Na_3Bi [21, 145] and Cd_3As_2 [23, 146, 147]. Due to non-zero Berry curvature, many novel physical properties such as giant AHE and giant anomalous Hall angle, chiral anomaly, anomalous Nernst effect will emerge in magnetic WSM, holding potential applications in spintronics field. In the early stage, several candidate materials were predicted, such as $R_2Ir_2O_7$ (R = Nd, Pr) [20], $HgCr_2Se_4$ [148]. Recent efforts have focused on $Co_3Sn_2S_2$ [136, 137] and Mn_3X (X = Sn, Ge) [138–140] which clearly host the band structure and transport characters as expected by magnetic WSM. We will briefly introduce these magnetic materials.

3.1 FeSn

FeSn crystallizes in a hexagonal structure ($P6/mmm$) with the Fe atoms forming a Kagome lattice [150, 151, 153, 154]. Like Fe_3Sn_2, FeSn is formed by interlacing Fe_3Sn layer and Sn layer. The difference is that there is only one Kagome layer (Fe_3Sn layer) in a unit cell [Fig. 6(a)]. It is closer to the 2D limit than Fe_3Sn_2. Below $T_N = 365$ K [Fig. 6(b)], the Fe spins form FM Kagome layers which are stacked antiferromagnetically along the c axis. The Dirac nodal line along the K–H line opens small energy gaps when SOC is considered, except at the H point where a gapless Dirac point (protected by PT and S_{2Z} symmetry) still exist, rendering FeSn as an AFM DSM. Such gapless Dirac cones have been directly observed by ARPES [150, 151] [Figs. 6(c, d)]. Besides, the flat band because of the Kagome layer has also been observed directly by ARPES [Fig. 6(e)]. Furthermore, in a planar tunneling spectroscopy measurement [152], an anomalous enhancement in tunneling conductance within a finite energy range of FeSn has been observed in its Schottky heterointerface with Nb-doped $SrTiO_3$ [Fig. 6(f)]. Such tunneling conductance peak is attributed to spin-polarized flat band localized at the FM Kagome layer at the Schottky interface.

3.2 $Co_3Sn_2S_2$

$Co_3Sn_2S_2$ crystallizes in the $R\bar{3}m$ space group with a stacking order –Sn–S–Co_3Sn–S– from top to bottom. The central Co layer forms a 2D Kagome lattice with one Sn atom at the center of the hexagon, as shown in Fig. 7(a). $Co_3Sn_2S_2$ is a ferromagnet with a curie temperature of 175 K and a magnetic moment of 0.3 μ_B/Co. In magnetization measurement, the saturation field along c axis is low (0.05 T) but along in-plane is

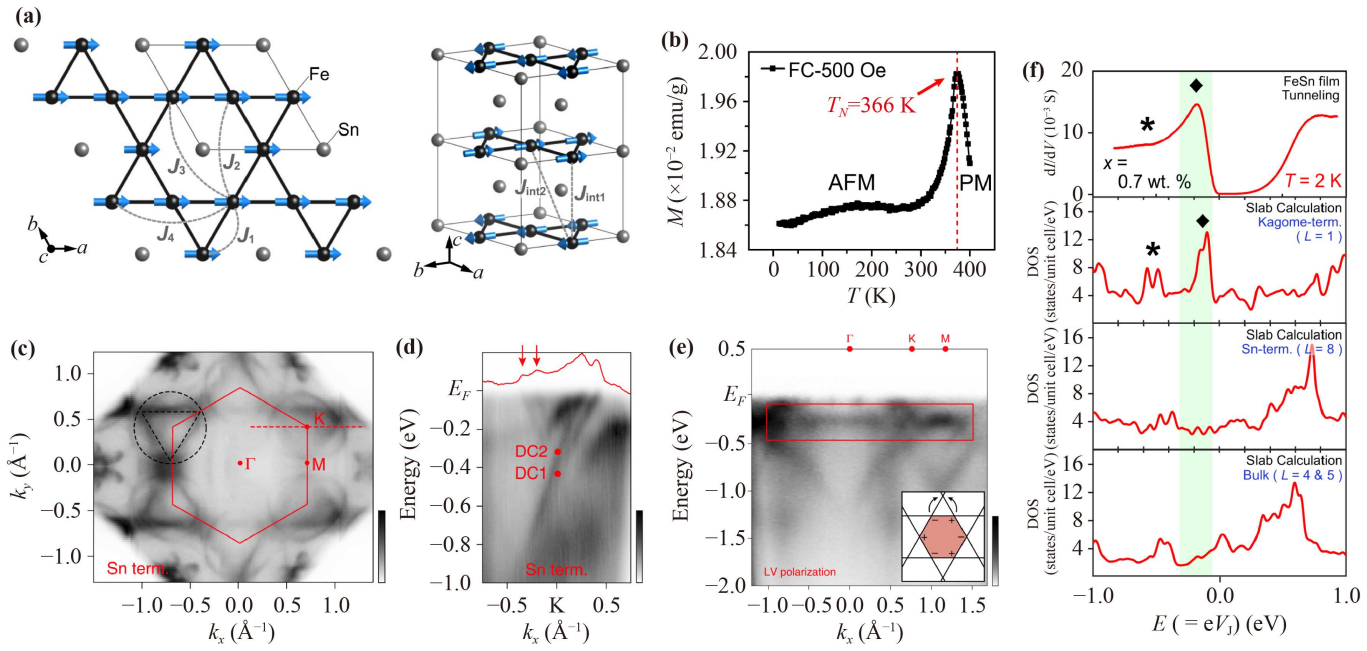

Fig. 6 **(a)** FeSn lattice structure and magnetic configuration, reproduced from Ref. [149]. **(b)** Magnetization as a function of temperature under field cooling (FC) with an applied magnetic field of 500 Oe, reproduced from Ref. [150]. **(c, d, e)** ARPES Fermi surface mapping and spectra reveal two Dirac cones features around K point (d) and flat band close to the Fermi level (e), reproduced from Ref. [151]. **(f)** Planar tunneling spectroscopy reveals an anomalous enhancement in tunneling conductance within a finite energy range of FeSn (black diamond), attributed to a spin-polarized flat band, reproduced from Ref. [152].

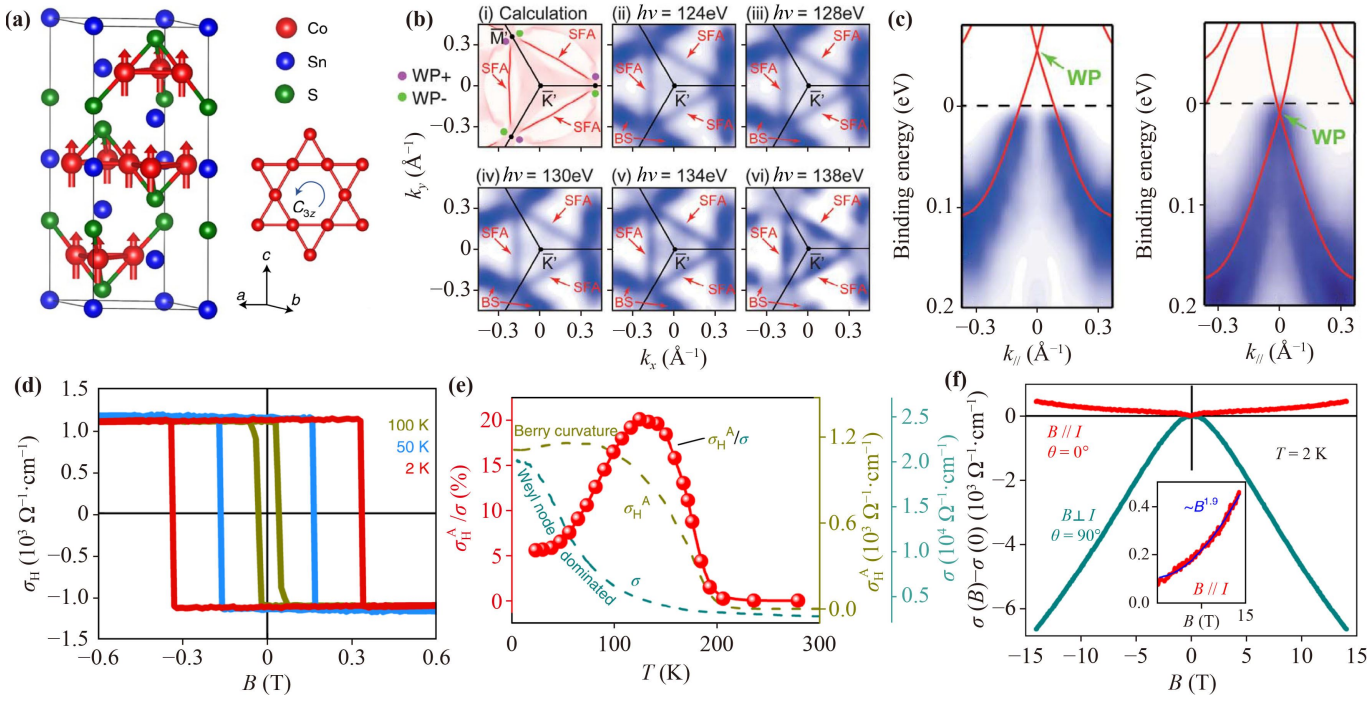

Fig. 7 **(a)** $Co_3Sn_2S_2$ lattice structure and magnetic configuration, reproduced from Ref. [48]. **(b)** Calculated Fermi surface (i) and experimental Fermi surfaces under different photon energies (ii–vi) around K′ points in $Co_3Sn_2S_2$, SFA: surface Fermi arc, BS: bulk state, reproduced from Ref. [137]. **(c)** Intrinsic band structure (left), and band structure after potassium dosing and from calculation (red lines) of $Co_3Sn_2S_2$, reproduced from Ref. [137]. **(d)** Field dependence of the Hall conductivity σ_H, reproduced from Ref. [48]. **(e)** Temperature dependences of the anomalous Hall conductivity (σ_H^A), the charge conductivity (σ) and the anomalous Hall angle (σ_H^A/σ) at zero magnetic field, reproduced from Ref. [48]. **(f)** Measured magnetoconductance for $B \perp I$ and $B//I$, reproduced from Ref. [48].

extremely high (> 9 T), confirming that the easy magnetic axis is c-axis [48, 155]. Combining theory and experiments, $Co_3Sn_2S_2$ is an ideal FM WSM with three pairs of Weyl points whose energies are only ~ 60 meV above the Fermi level [136, 137, 156–161]. The Weyl nodes have been observed by ARPES after doping alkaline metal [Fig. 7(c)]. Three Fermi arcs form a triangular-like loop around the K′ point near Fermi surface. Meanwhile, the electronic structure does not undergo obvious dispersion along the k_z direction, suggesting the nature of TSSs [Fig. 7(b)]. Termination-dependent surface band structures of $Co_3Sn_2S_2$ were observed by using STM [136]. Different surface potentials imposed by three different terminals will change the Fermi arc contour and Weyl node connectivity. On the Sn-termination, the Fermi arcs connect Weyl nodes within the same Brillouin zone, while on the Co-termination, the connectivity spans the two adjacent Brillouin zones. On S-termination, Fermi arcs overlap with the trivial surface-projected bulk bands. The topologically protected and unprotected electronic properties of WSMs $Co_3Sn_2S_2$ were verified.

According to first-principles calculation, the Weyl nodes in $Co_3Sn_2S_2$ locate close to the Fermi level and produce a giant anomalous Hall conductivity (AHC) (~1100 $\Omega^{-1}\cdot cm^{-1}$), which has been directly observed in transport measurement [Figs. 7(d, e)] [48, 161, 162]. Besides, giant anomalous Hall angle also emerges in this material. As shown in Fig. 7(e), with increasing temperature, a maximum value of nearly 20% is reached around 120 K, which is at least one order of magnitude higher than that of conventional magnetic materials. Negative magnetoresistance is found in $Co_3Sn_2S_2$, as shown in Fig. 7(f), when the magnetic field is applied in the in-plane direction, the longitudinal resistance is negative, and when the external magnetic field is applied in the out-of-plane direction, the longitudinal resistance changes from negative to positive, showing evidence of chiral anomaly [48, 155, 161, 162]. In $Co_3Sn_2S_2$ thin film, a maximum Nernst thermopower of 3 $\mu V\cdot K^{-1}$ is achieved [50], demonstrating the possibility of application of hard magnetic topological semimetals for low-power thermoelectric devices.

3.3 Mn_3X (X = Sn, Ge)

Mn_3X (X = Sn, Ge) has a hexagonal Ni_3Sn-type structure and crystalizes in the $P6_3/mmc$ space group. One unit cell consists of two sets of Mn layers stacked along c-axis and each Mn layer forms a breathing-type Kagome lattice with one Sn atom at the center of the hexagon, as shown in Fig. 8(a). Mn_3Sn and Mn_3Ge are both chiral antiferromagnets which means Mn moments are forming a 120° ordering with a negative vector chirality [Fig. 8(b)] [164, 165]. The AFM transition temperature of Mn_3Sn and Mn_3Ge is 430 K and 372 K, respectively. Because the electronic structures of Mn_3Sn and Mn_3Ge are quite similar and the study of Mn_3Sn is more comprehensive, we will mainly focus on Mn_3Sn. Mn_3Sn possesses non-collinear AFM spin texture and strong SOC effect, which produce multiple pairs of Weyl points close to the Fermi level, according to first-principal calculation [138, 166, 167] [Fig. 8(c)]. However, ARPES

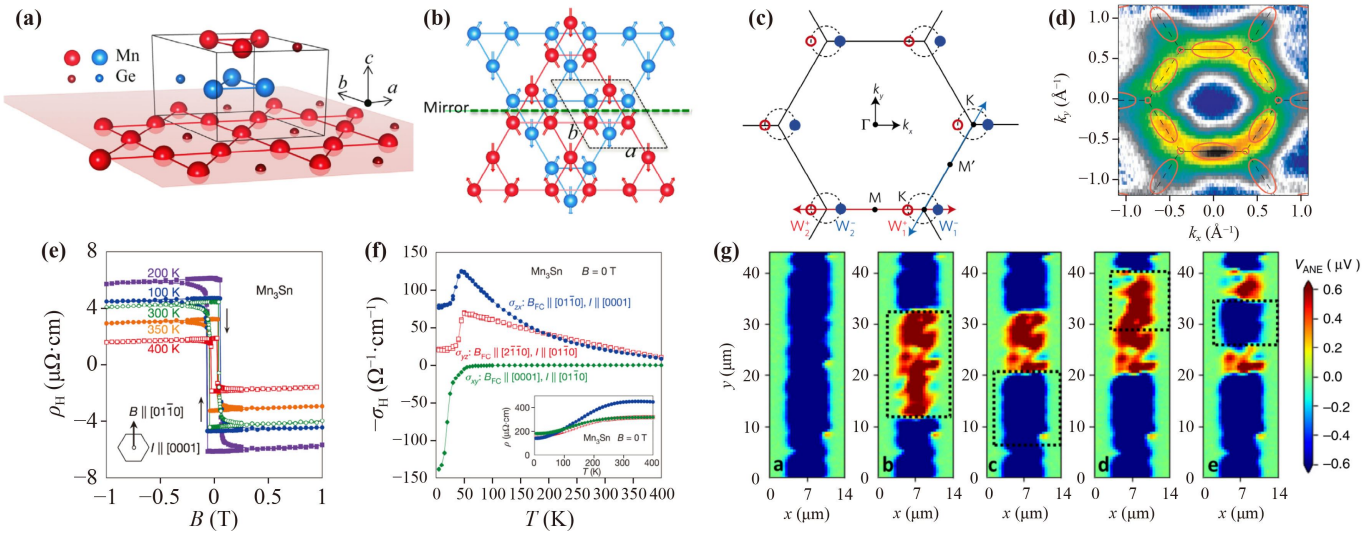

Fig. 8 **(a)** Mn_3Ge lattice structure and **(b)** magnetic configuration, reproduced from Ref. [139]. **(c)** Band structure calculation reveals the existence of one pair of Weyl points close to the Fermi level around K points in Mn_3Sn, reproduced from Ref. [138]. **(d)** Fermi surface mapped by ARPES and from calculation (purple curves) of Mn_3Sn, reproduced from Ref. [138]. **(e, f)** Field dependent Hall resistance at different temperatures show AHE behavior and temperature dependent zero-field component of the AHE in Mn_3Sn, reproduced from Ref. [140]. **(g)** Anomalous Nernst voltage V_{ANE} image mapped by scanning thermal gradient microscopy reveal the existence of magnetic domain and domain writing, reproduced from Ref. [163].

spectra [138] measured on Mn_3Sn lacks clear features of quasiparticle bands, likely due to strong correlation effect of Mn 3*d* electrons [Fig. 8(d)].

Novel transport properties governed by the topological nature can serve as evidence for Weyl fermions. In Mn_3Sn, strongly anisotropic magnetoconductance was observed. The sign of magnetoconductance changed when rotated the direction of magnetic field from being parallel to perpendicular to the current direction, serving as strong evidence of chiral anomaly [138, 164]. The large AHE is also a key characteristic of magnetic WSM. In the traditional sense, because the magnetic configuration of Mn_3Sn is AFM, there is no net magnetic moment in this material and the AHE will not emerge. But many reports revealed that Mn_3Sn exhibits a large AHE [139, 140, 166, 168–171]. Figures 8(e, f) show the temperature-dependence of zero-field Hall conductivity under different magnetic field and current directions [140]. We can see that when the magnetic field and the current are applied along the $(01\bar{1}0)$ and (0001) direction, the σ_H will achieve a maximum value of nearly 130 $\Omega^{-1}\cdot cm^{-1}$ at 50 K. In Mn_3Ge, by employing similar magnetic field and current direction, even higher AHC have been obtained [139, 168]. The large AHE in Mn_3X is mainly caused by the non-zero Berry curvature produced by Weyl nodes [164]. Besides chiral anomaly and large AHE, many other exotic physical properties such as large anomalous Nernst effect [163, 164, 172–174], planer Hall effect [171, 175, 176], magnetic spin Hall effect and magnetic inverse spin Hall effect [177] are also observed in Mn_3X. Furthermore, as shown in Fig. 8(g), anomalous Nernst voltage V_{ANE} image mapped by scanning thermal gradient microscopy reveals the existence of magnetic domains. The orientation of these domains can be changed (written) by laser-induced local thermal gradient [163], offering a chance to study spintronics phenomena in non-collinear antiferromagnets with spatial resolution.

3.4 Co_2MnGa

A new family of magnetic WSM emerged among the magnetic Heusler alloys, i.e., the Heusler alloy WSMs [181, 182]. It is an important family due to their rich transport properties and several superiorities. Firstly, the Curie temperatures of most Heusler compounds are above the room temperature [183, 184]. Secondly, this

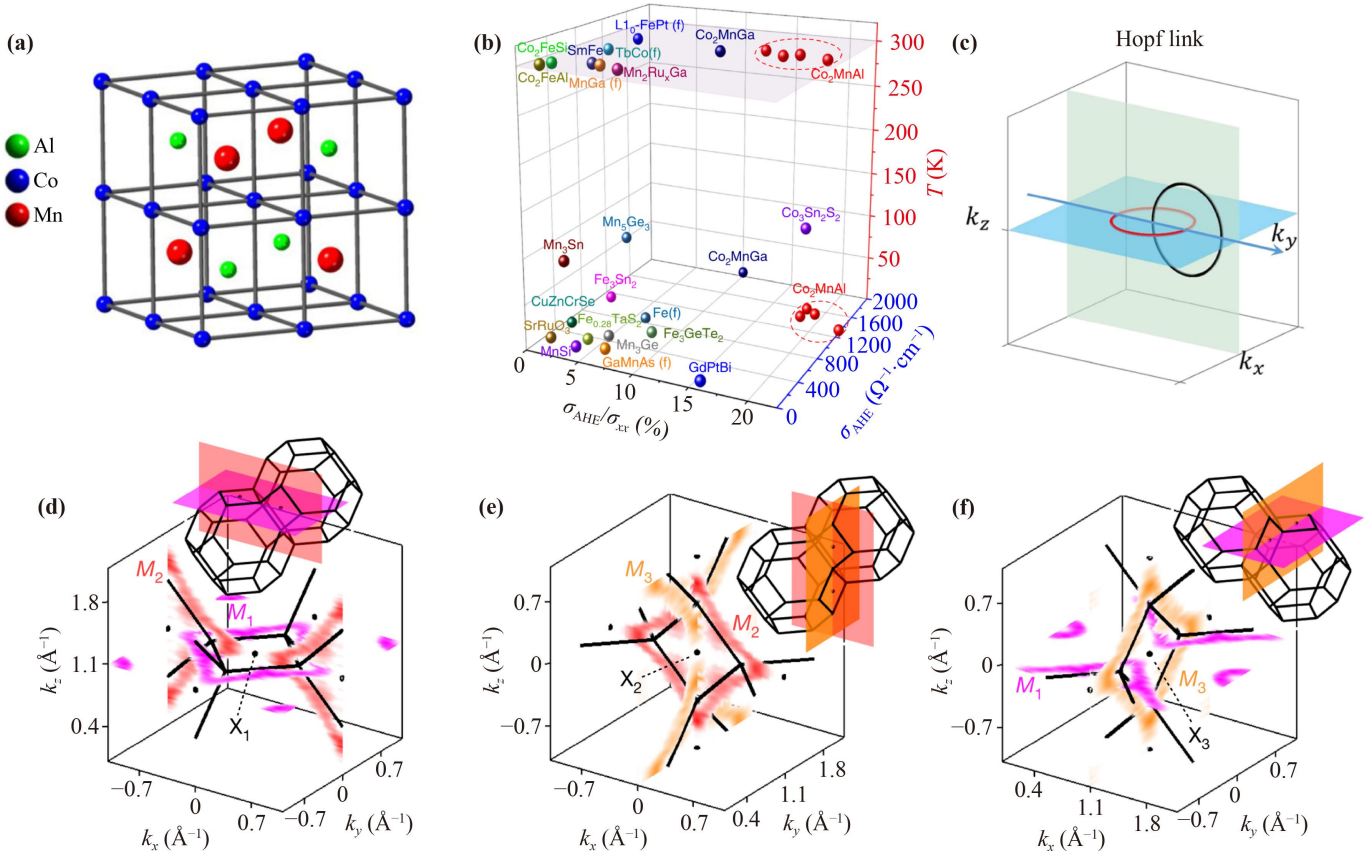

Fig. 9 **(a)** Crystal structure of Co_2MnAl [178]. **(b)** Comparison of anomalous Hall angle $\tan\Theta^H=\sigma_{AHE}/\sigma_{xx}$ and anomalous Hall conductivity σ_{AHE} between Co_2MnAl and other magnetic conductors [178]. **(c)** Hopf link which consists of two rings on the mirror planes and intertwined each other [179]. **(d–f)** Linked Weyl loops in Co_2MnGa [180]. M1- and M2-loop Fermi surfaces plotted in adjacent bulk Brillouin zones (d). Same as (d) but for the M2- and M3-Fermi surfaces (e) and the M1- and M3-Fermi surfaces (f).

kind of materials has a significant AHE and spin Hall effect arising from the large Berry curvature [179, 181, 182, 185–187]. Thirdly, Heusler compounds are usually soft magnetic materials, which means that their magnetization direction can be tuned by a weak magnetic field. These properties facilitate spin manipulation and applications in spintronics, as a result, these Heusler alloy WSMs have been widely studied.

As full Heusler compounds, Co-based Heusler materials have the formula of Co_2XZ (X = IVB or VB; Z = IVA or IIIA), here we focus on Co_2MnGa and Co_2MnAl. Co_2MnGa (Co_2MnAl) crystalizes in a face-centered cubic Bravais lattice (space group $Fm\bar{3}m$, No. 225), as shown in Fig. 9(a). The relevant symmetries are the three mirror planes and three C_4 rotation axes. The Curie temperature of Co_2MnGa and Co_2MnAl are known to be ~700 K [179] and 726 K [183], respectively. Transport experiments showed that Co_2MnAl has a giant room-temperature AHE with the Hall angle (Θ^H) reaching a record value $\tan\Theta^H = 0.21$ at the room temperature among magnetic conductors [178], as shown in Fig. 9(b). This property results from the gapped nodal rings that generate large Berry curvature. Furthermore, for Co_2MnGa films, when the E_F is set in the magnetization-induced gap of the Weyl cones by the electronic doping, the highest anomalous Nernst thermopower of a record value 6.2 $\mu V \cdot K^{-1}$ will be reached at room temperature [188].

The Hopf link is originally a mathematical concept which consists of two rings on the two perpendicular planes, each passing through the center of each other, as shown in Fig. 9(c). The symmetry of Co_2MnGa can protect this band crossing associated with the unusual linking-number (knot theory) invariant, giving rise to a variety of new types of topological semimetals [179, 180, 185–187, 189–192]. Systematic ARPES investigation of the electronic structure of Co_2MnGa has been carried out and directly revealed three intertwined degeneracy loops in the material's three-torus bulk Brillouin zone [Figs. 9(d–f)]. In addition, the Seifert boundary states protected by the bulk-linked loops have been predicted and observed, while the links and knots in the electronic structure and the accompanied exotic behaviors remain unexplored.

3.5 EuB_6

The EuB_6 crystallizes in a similar body-centered-cubic-

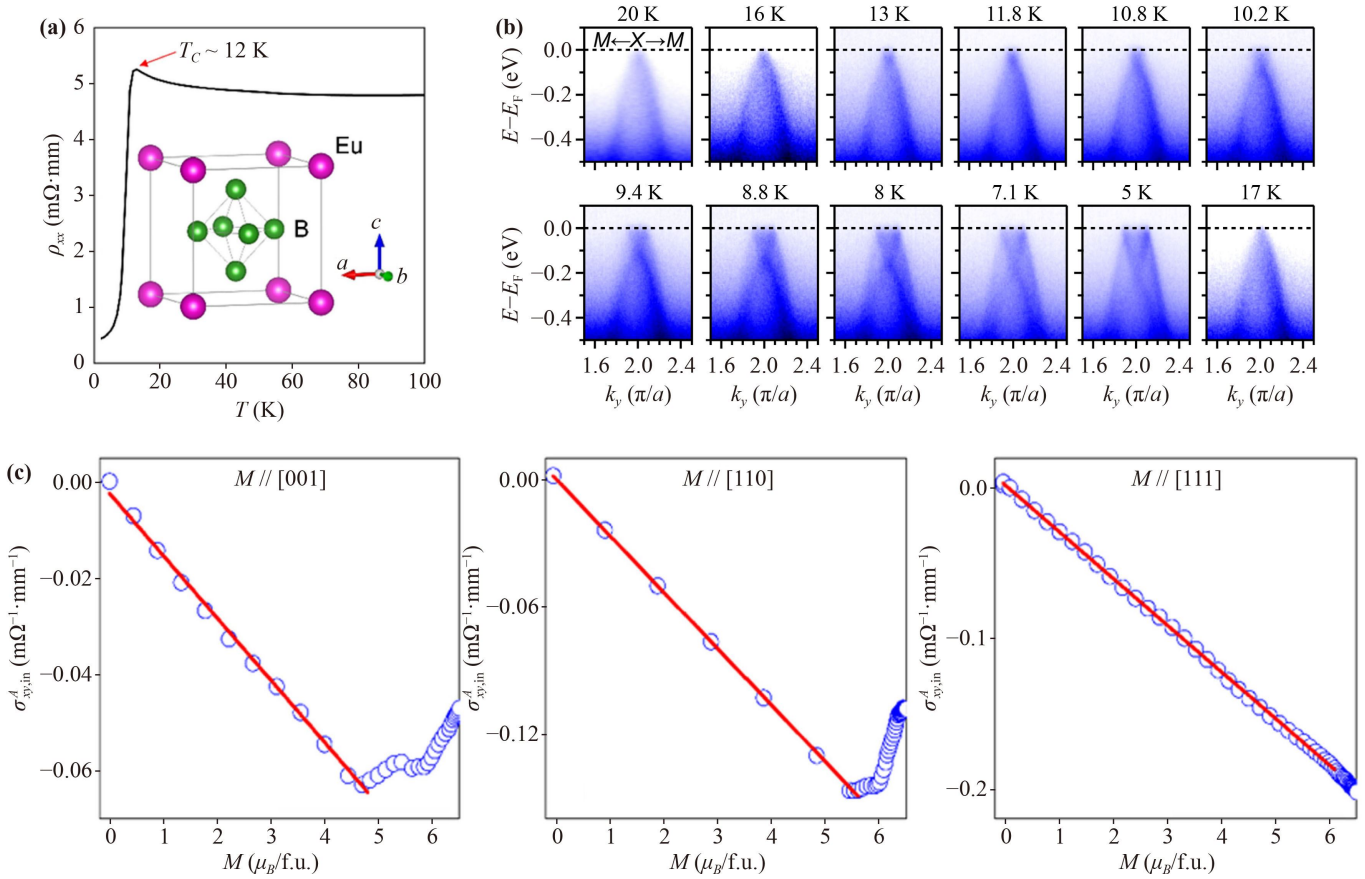

Fig. 10 **(a)** Crystal structure of EuB_6 and its longitudinal resistivity as a function of temperature [193]. **(b)** Temperature dependent band structure of B-terminated surface along M–X, which is taken with $h\nu = 135$ eV [194]. **(c)** The intrinsic anomalous Hall conductivity as a function of different magnetization at 2 K [193].

like crystal structure with space group $Pm\bar{3}m$ (No. 221) [Fig. 10(a)]. EuB_6 is a soft FM semimetal which has a very small magnetic anisotropy energy so that the magnetization can be easily modulated by magnetic field [193, 195–197]. Electronic transport and magnetic susceptibility measurements showed that the system undergoes a paramagnetic to FM phase transition at about 15.3 K and a new FM phase manifests below about 12.5 K with moment oriented to the (111) direction [198–200]. The magnetotransport properties of EuB_6 have been widely studied around magnetic phase transition point, such as the metal-insulator transition, colossal magnetoresistance and quantum nematic phase [201–203].

It has been predicted that EuB_6 is a topological nodal-line semimetal when the magnetic moment is aligned along the (001) direction, and it turns out to be a WSM with three pairs of Weyl nodes when rotating the magnetic moment to (111) direction. Specifically, when the moment is in the (110) direction, a composite semimetal phase featuring the coexistence of a nodal line and Weyl points manifests [195]. The electronic structures on the two different cleavage planes in EuB_6, i.e., the Eu- and B-terminated surfaces, have been investigated [194, 204]. For the B-termination, in the FM state, obvious Zeeman splitting occurs for both the conduction and valence bands, which gives rise to the overlap of subbands and thus the band inversion at the time-reversal point X of the Brillouin zone [Fig. 10(b)]. In this case, EuB_6 enters a topological semimetal state with an ideal electronic structure near E_F. The topological properties can be investigated by measuring the magnetotransport properties due to the correlation between the band structure and the local moments. Figure 10(c) shows the intrinsic anomalous Hall conductivity as a function of magnetization with different directions at 2 K [193]. An intrinsic large anisotropic magnetoresistance of –18% at 0.2 T was observed and interpreted as the modification from the Berry curvature in a tilted Weyl cone [205]. The theoretical prediction that a large-Chern-number QAH effect could be realized in its (111)-oriented quantum-well structure [195] needs further investigations.

3.6 Fe_3GeTe_2

Fe_3GeTe_2 crystallizes in a hexagonal structure ($P6_3/mmc$, No. 194) in which the layered Fe_3Ge substructure are sandwiched by two layers of Te atoms [Fig. 11(a)]. Fe_3GeTe_2 is FM with Fe moments along the c axis and a Curie temperature of 204–230 K [Fig. 11(b)] [206, 211–213]. ARPES measurements have revealed two pockets around Γ point and one at K point [Fig. 11(c)]. Temperature-dependent ARPES spectra exhibits a massive spectral weight transfer in the FM state induced by exchange splitting [207]. Orbital-driven nodal line along K–H protected by crystalline symmetry has been predicted [Fig. 11(f)]. Introducing SOC will gap the nodal line and generate large Berry curvature [210], an effective source of a large AHE in Fe_3GeTe_2. We note that Fe_3GeTe_2 is considered as a gapped nodal line semimetal with the Weyl point awaiting verification.

Fe_3GeTe_2 also contains very rich physical properties.

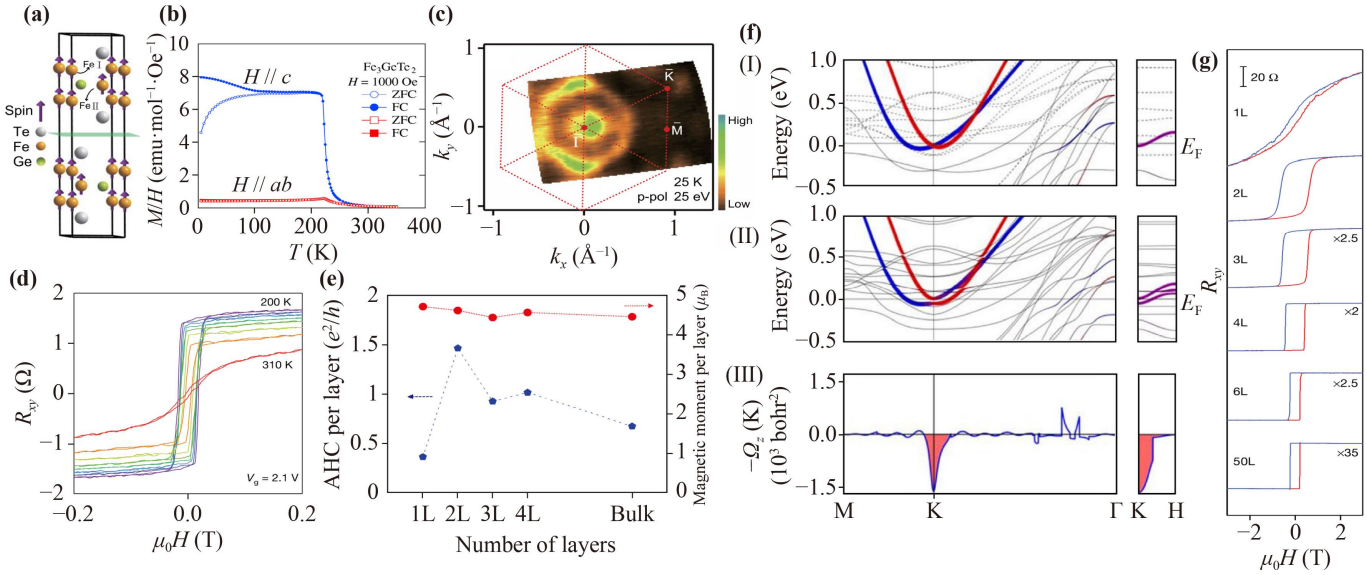

Fig. 11 **(a)** Fe_3GeTe_2 lattice structure, magnetic configuration and **(b)** magnetic properties, reproduced from Refs. [206, 207]. **(c)** ARPES measured Fermi surface of Fe_3GeTe_2, reproduced from Ref. [207]. **(d)** Hall resistance of a four-layers Fe_3GeTe_2 flake [208]. **(e)** The dependence of AHC and magnetic moment per layer on the number of layers, reproduced from Ref. [209]. **(f)** Calculated electronic structures of Fe_3GeTe_2 without (I) and with (II) SOC. Majority spins: solid. Minority spins: dashed. (III) Calculated Berry curvature along the symmetry lines, reproduced from Ref. [210]. **(g)** Hall resistance with varying numbers of layers [208].

Due to the gapped nodal line, negative magnetoresistance [214, 215], anomalous Nernst effect [216] and AHE were observed [209, 210, 213]. Compared with other itinerant FM materials, Fe_3GeTe_2 has both large anomalous Hall factor and anomalous Hall angle [Figs. 11(d, e)]. Due to the weak interlayer coupling, Fe_3GeTe_2 can be exfoliated into sheets with different number of layers. More importantly, its novel transport and magnetic properties show stability at room temperature and dependence on the number of layers, interlayer coupling and carrier density [208, 209, 217–223], holding potential in spintronics applications.

3.7 $EuCd_2As_2$

$EuCd_2As_2$ belongs to EuM_2X_2 (M = metal; and X = Group 14 or 15 element) family in which several members are studied as magnetic TI candidates (see Section 2). The exact band structure details and topological phase are sensitively related to the magnetic configuration. The crystal structure of $EuCd_2As_2$, with space group 164 ($P\bar{3}m1$), is shown in Fig. 12(a). The Eu atoms form a simple hexagonal lattice at the 1a Wyckoff position. The As and Cd atoms at the 2b positions form the other four atomic layers with the sequence of –Cd–As–Eu–As–Cd– along the c axis [224, 229, 230]. Eu moments prefer an intralayer FM coupling and an interlayer AFM coupling along the c axis, i.e., an A-type AFM, which doubles the unit cell along the c direction. Figures. 12(b) and (c) show two such magnetic configurations by showing Eu atoms with magnetic moment directions along c (A-type AFMc) and along a (A-type AFMa). A-type AFMc is proposed based on the anisotropic magnetic and transport properties [224, 229]. A-type AFMa is proposed based on the resonant elastic X-ray scattering [225, 231], first-principles calculations [232] and magnetostriction measurements [233]. Furthermore, neutron diffraction on isotopic ^{153}Eu and ^{116}Cd revealed a $k = (0, 0, 0)$ FM order at zero field with the Eu moments pointing along the in-plane (210) direction with a $\sim 30°$ out-of-plane canting [magnetic space group $C2'/m'$, Fig. 12(d)] [226].

According to the first-principles calculation and symmetry analysis, various topological phases emerge based on different magnetic configurations in $EuCd_2As_2$. For A-type AFMz, DSM phase exists with the gapless Dirac point protected by the PTL symmetry operation which is the product of inversion symmetry P, time reversal symmetry T and crystalline translation symmetry L [227, 234]. For A-type AFMx, spin configuration breaks the C_3 symmetry in the AFM state of $EuCd_2As_2$ and leads to an axion insulator with a hybridization gap of ~1 meV. Massless Dirac surface states appear on some surfaces protected by the mirror or TL symmetries. For other surfaces without such symmetry, the surface states are gapped and the hinge states, associated with higher order TI states, emerge at the edges [126, 235]. There are other calculations which predict $EuCd_2As_2$ as a WSM with a single pair of Weyl points very close to the Fermi level [226, 230, 236]. Such Weyl phase can be generated in $EuCd_2As_2$ by applying a magnetic field

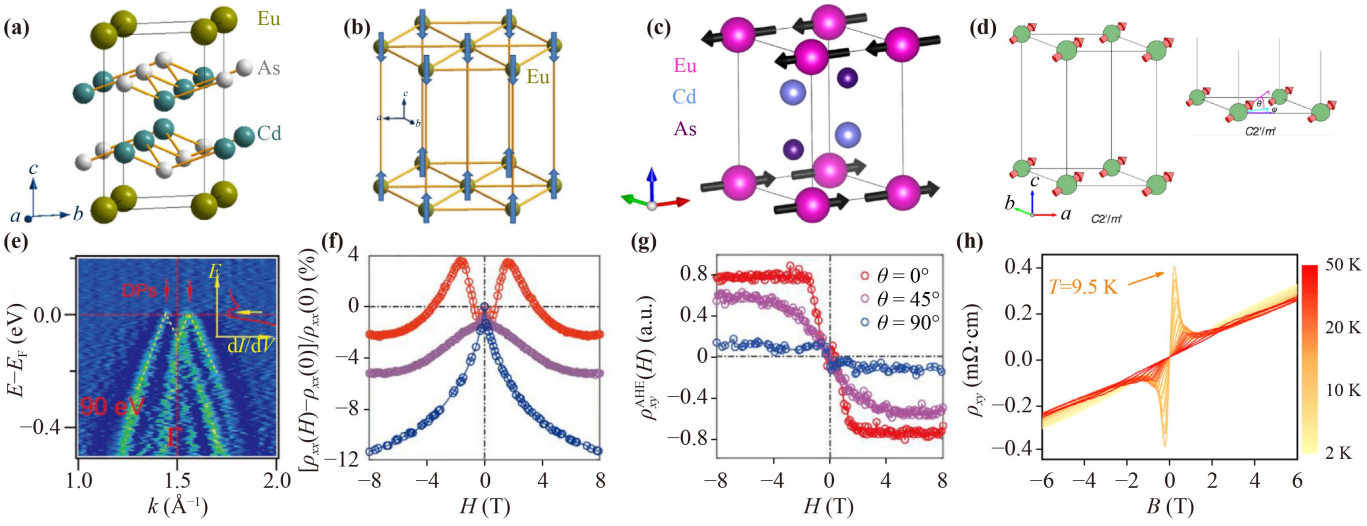

Fig. 12 **(a)** Crystal structure of $EuCd_2As_2$, from [224]. **(b)** Proposed A-type AFM structure on Eu sites with the moments lying out-of-plane, from [224]. **(c)** Proposed A-type AFM structure with the moments lying in-plane, from [225]. **(d)** Best-fit magnetic structure from neutron diffraction measurement with moments along the (210) direction with 30° canting, from [226]. **(e)** ARPES spectral along $Z-\Gamma-Z$ presents an "M"-shaped feature around Γ, from [227]. **(f, g)**, Negative magnetoresistance and anomalous Hall resistance with three different orientations between H and E, from [226]. **(h)** Magnetic-field dependence of the Hall resistivity at different temperatures shows giant nonlinear behavior, from [228].

> 1.5 T along the c axis [236] or alloying with Ba at the Eu site to stabilize the FM configuration [230]. In fact, the recently confirmed spin-canted structure as shown in Fig. 12(d) naturally hosts such WSM phase [226]. Spectroscopically, ARPES measurements have observed linear band crossings at the Fermi level and especially an "M"-shaped feature around Γ point [Fig. 12(e)], suggesting a nontrivial band inversion. Such features cannot distinguish between the semimetal and insulator phase as the gap is only ~1 meV, comparable to the thermal broadening effect at ~3 K. ARPES or scanning tunneling spectroscopy measurements at ultralow temperature are needed. Spin-resolved ARPES is also useful to examine the spin degeneracy of these linear bands and crossings.

Magnetic transport experiments have provided more information on the interplay between magnetism and band topology in $EuCd_2As_2$. Negative magnetoresistance [Fig. 12(f)], as signature of chiral anomaly is observed along with AHE [Fig. 12(g)] [225, 226, 228]. These transport results support as-grown $EuCd_2As_2$ in a semimetal phase, yet gate tunable transport is needed to verify the absence of gap close to the Fermi level. It was further reported that the Hall resistance shows a giant nonlinear behavior originating from a series of magnetic-field-induced Lifshitz transitions in the spin-dependent band structure [Fig. 12(h)] [228]. Combined with band structure calculation, these results suggest that in $EuCd_2As_2$, electronic structure is extremely sensitive to the spin canting angle, with the magnetic field causing band crossing and band inversion and introducing a band gap when oriented along specific directions, offering an ideal platform for Berry curvature engineering.

4 Other magnetic topological metals

As introduced in the previous section, intrinsic magnetic TIs have nontrivial bulk band topology featured by a global bulk gap and TSS residing inside the bulk gap. Chemical potential can be tuned into the bulk gap to eliminate the transport contribution from the bulk bands, a key prerequisite to realize quantized Hall transport. There exist other magnetic systems which lack a global bulk gap in the whole momentum space but possess a locally nontrivial bulk gap and TSS inside. Such systems always exhibit metallic transport behavior contributed by trivial bulk bands. AHE is generally expected from the coexisting net magnetic moment and locally nontrivial topology. We term such materials as magnetic topological metals. It is noted that there is no strict theoretical scheme describing magnetic topological metal since the metallicity does not only come from band-topology-induced TSS but rather the trivial bulk bands. We choose this term only to emphasize its distinction from intrinsic magnetic TIs and topological SMs.

4.1 Fe_3Sn_2

Fe_3Sn_2 is a layered Kagome compound with a space group of $R\bar{3}m$ formed by interlacing two Fe_3Sn layers and one Sn layer. The Fe atoms in the Fe_3Sn layer form a Kagome structure, and the Sn atoms exhibit a honeycomb structure. The Sn atomic layer also exhibits a honeycomb distribution [Fig. 13(a)] [239]. Fe_3Sn_2 is FM in the ground state with a Curie temperature of T_C ~

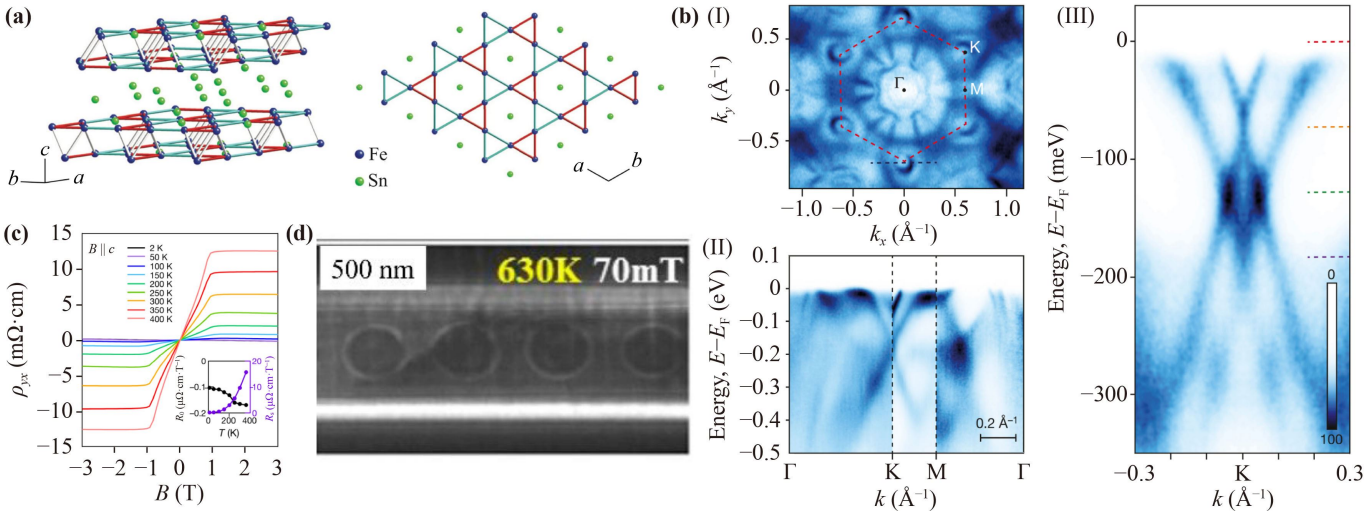

Fig. 13 **(a)** Crystal structure schematic of Fe_3Sn_2, reproduced from Ref. [237]. **(b)** Fermi surface (I), high symmetry line band structure (II) and gapped Dirac cones at K point (III), reproduced from Ref. [238]. **(c)** Field dependent Hall resistivity and the extracted ordinary and anomalous Hall coefficients, reproduced from Ref. [238]. **(d)** Under-focused Lorentz transmission electron microscopy images of skyrmionic bubbles in the 600 nm nanostripe taken at temperature 630 K with magnetic field 70 mT.

610 K [237, 240–242]. Due to the weak binding force between layers, Fe_3Sn_2 produces three different cleavage planes, Fe_3Sn-1-termination, Fe_3Sn-2-termination, and Sn-termination [238, 243]. The experimentally observed band structures mainly come from Fe_3Sn-1-termination. The shape of the Fermi surface confirms the trigonal structure of Fe_3Sn_2. ARPES measurements have revealed two Dirac cone features at the corner of Brillouin zone, which are gapped by the SOC effect [Fig. 13(b)]. Such strong SOC also couples the magnetic and electronic structure of Kagome lattice, exhibiting a magnetization-driven giant nematic (two-fold-symmetric) energy shift [244]. In the Kagome lattice, the destructive interference of the electron Bloch wave function can effectively localize the electrons to produce flat bands. Such flat bands are observed in Fe_3Sn_2, which are ~ 0.2 eV below the Fermi level [243].

The coexistence of nontrivial band topology and FM order in Fe_3Sn_2 produces giant AHE [40, 238, 245]. The measured AHC is found to be temperature independent and persists above room temperature [Fig. 13(c)], which is suggestive of prominent Berry curvature from the time-reversal-symmetry-breaking electronic bands of the Kagome plane. Moreover, Fe_3Sn_2 shows complex magnetic bubbles and magnetic vortex structure like skyrmions [246–251]. These bubbles are 3D magnetic domains with complicated evolution of spin texture, which not only give rise to topological Hall transport response, but also show record-high temperature stability in magnetic racetrack memory devices [Fig. 13(d)].

4.2 RT_6X_6 (R = Rare earth metal; T = transition metal; X = Sn, Ge)

Layered Kagome compounds RT_6X_6 (R = rare earth metal, T = transition, alkali, alkaline earth metal, X=Sn or Ge) crystallize in the $P6/mmm$ space group. As shown in Fig. 14(a), T_3X is the Kagome layer of T ions with one X atom at the center of the hexagon. In RX layer, the R atom lies at the center of the hexagons surrounded by the X atoms. X layer is a hexagonal layer only consisting of X atoms and separating each unit cell. In this system, the 4f electrons in the R element interact with the 3d electrons in the transition metal element T to generate a rich magnetic structure. Many novel physical properties are also found in this system, such as flat band, giant AHE and Nernst effects. Recent published articles focus mostly on RMn_6Sn_6 and RV_6Sn_6. Therefore, the following content will discuss these two systems.

Since Mn is a well-known magnetic metal, there are many magnetic configurations emerged due to the interaction between Mn 3d magnetic moment and R 4f magnetic moments [Figs. 14(b, e)] [252, 255–258]. When R is a lanthanide element (R = Gd–Tm, Lu), its magnetic configuration varies from FM to AFM. For R = Gd to Ho, their magnetic configuration is ferrimagnetic, and for R = Er, Tm and Lu, they possess AFM ground state. The direction of the magnetic moment of the R element tends to be antiparallel to the magnetic moment of Mn, and the moment direction is variable for different R elements. $GdMn_6Sn_6$ moment is arranged in-plane, and $TbMn_6Sn_6$ moment is arranged out-of-plane. $DyMn_6Sn_6$ and $HoMn_6Sn_6$ possess a conical magnetic

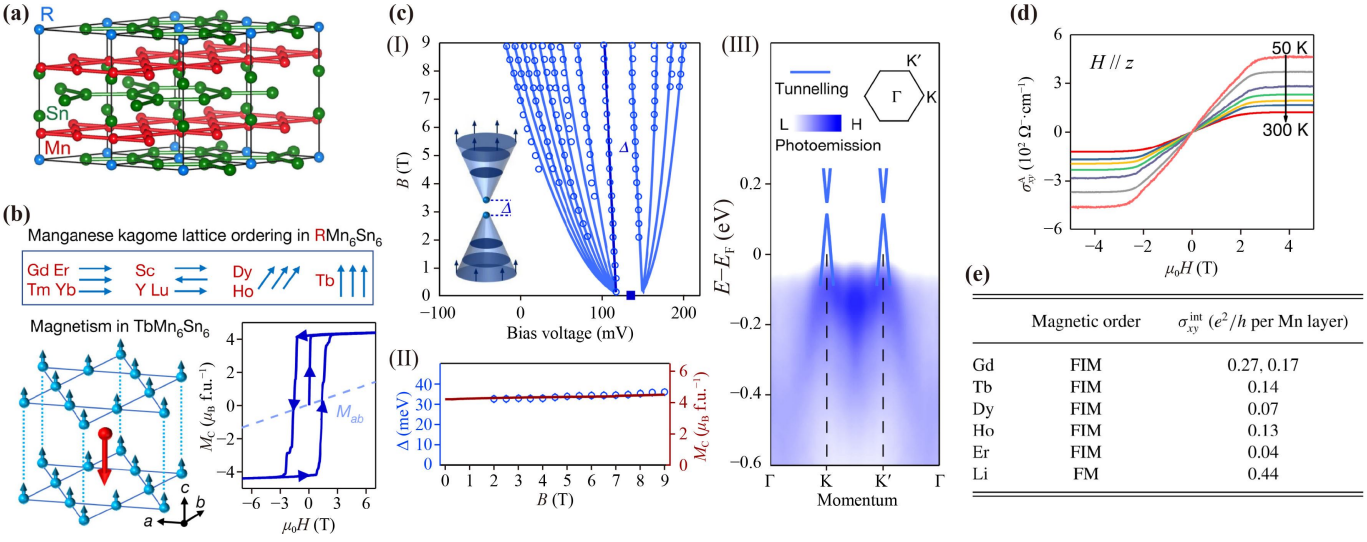

	Magnetic order	σ_{xy}^{int} (e^2/h per Mn layer)
Gd	FIM	0.27, 0.17
Tb	FIM	0.14
Dy	FIM	0.07
Ho	FIM	0.13
Er	FIM	0.04
Li	FM	0.44

Fig. 14 **(a)** RMn_6Sn_6 lattice structure comprised of different layers of Mn_3Sn, RSn, and Sn atoms, from [252]. **(b)** Magnetic structure of RMn_6Sn_6 with the direction of magnetic moments depending on the R site element, from [253] **(c)** Fitting the Landau fan data from field dependent scanning tunneling spectroscopy measurements on $TbMn_6Se_6$ (open circles) with the spin polarized and Chern gapped Dirac dispersion (solid lines) (I) resulting field dependent size of the Dirac gap (II). Such gap is located above the Fermi level as indicated by the ARPES spectra in (III), from [253]. **(d)** Temperature dependent AHC of $LiMn_6Sn_6$ for magnetic field parallel to the z axis, from [254]. **(e)** Comparison of the intrinsic AHC of $LiMn_6Sn_6$ with those of RMn_6Sn_6, where FIM denotes the ferrimagnet and FM is the ferromagnet, from [254].

structure. When R is Er and Tm, the Mn and Er = Tm sublattices are independently ordered in an AFM manner because the strength of the magnetic coupling is weak. Since there is no 4f electrons in Lu and Y, they form in-plane FM and helical AFM along c-axis. For R = Gd to Ho, the Curie temperature of them is 435, 423, 393, and 376 K, respectively. For R = Er to Lu and Y, the Neel temperature of them is 352, 347, 353, and 333 K, respectively. In general, the electronic structure is closely related to magnetic configuration, when magnetic configuration change, the electronic structure will also change. However, for the RMn$_6$Sn$_6$ (R = Gd–Tm, Lu, Y) system, even for the different R, the band structure does not change significantly, indicating weak coupling between the low energy bands and magnetic moments.

Kagome lattice usually hosts three typical band features: flat band over the whole Brillouin zone, Dirac cones located at the Brillouin zone corners, and the saddle points located at the Brillouin zone boundary. Such features have indeed been observed in YMn$_6$Sn$_6$ and others by ARPES [259, 260]. The strong correlation between magnetism and Kagome lattice can produce many novel physical properties. In TbMn$_6$Sn$_6$, its Kagome lattice features an out-of-plane magnetic ground state, so it is predicted to support the intrinsic Chern topological phase. In STM measurement, the Dirac cone with a Chern gap [Fig. 14(c)] and topological edge state are detected, implying its non-trivial topological nature [253].

The coexistence of nontrivial band topology and variation of magnetic structure results in novel transport behavior. In YMn$_6$Sn$_6$, a large room temperature anomalous transverse thermoelectric effect of ≈ 2 μV·K^{-1} is realized, larger than all canted AFM material studied to date at the room temperature [261]. In addition, topological Hall effect is observed in the transverse conical spiral phase of YMn$_6$Sn$_6$ and ErMn$_6$Sn$_6$ with similar magnetic configuration [262–264]. Large anomalous Hall conductivity is also observed in many RMn$_6$Sn$_6$ compounds such as LiMn$_6$Sn$_6$, TbMn$_6$Sn$_6$, DyMn$_6$Sn$_6$, and HoMn$_6$Sn$_6$, as shown in Figs. 14(d, e) [252, 254, 258, 262, 264].

In isostructural RV$_6$Sn$_6$ compounds, V atoms have no magnetic moments, so that RV$_6$Sn$_6$ magnetic configuration is different from RMn$_6$Sn$_6$. The magnetic configuration is determined to be out-of-plane AFM for R = Tb–Ho and in-plane AFM for R = Er and Tm. because Lu and Y also possess no magnetic moment, so the compounds for R = Lu and Y are PM metals [265]. Typical band features such as Dirac cone, saddle point, and flat bands are also observed in this family [266]. Furthermore, TSS Dirac cones emerge from the nontrivial bulk band topology and can be tuned in binding energy via potassium deposition [267].

4.3 EuAs$_3$

EuAs$_3$ crystallizes in a monoclinic structure (space group $C2/m$, No. 12). As shown in Fig. 15(a), the moments of

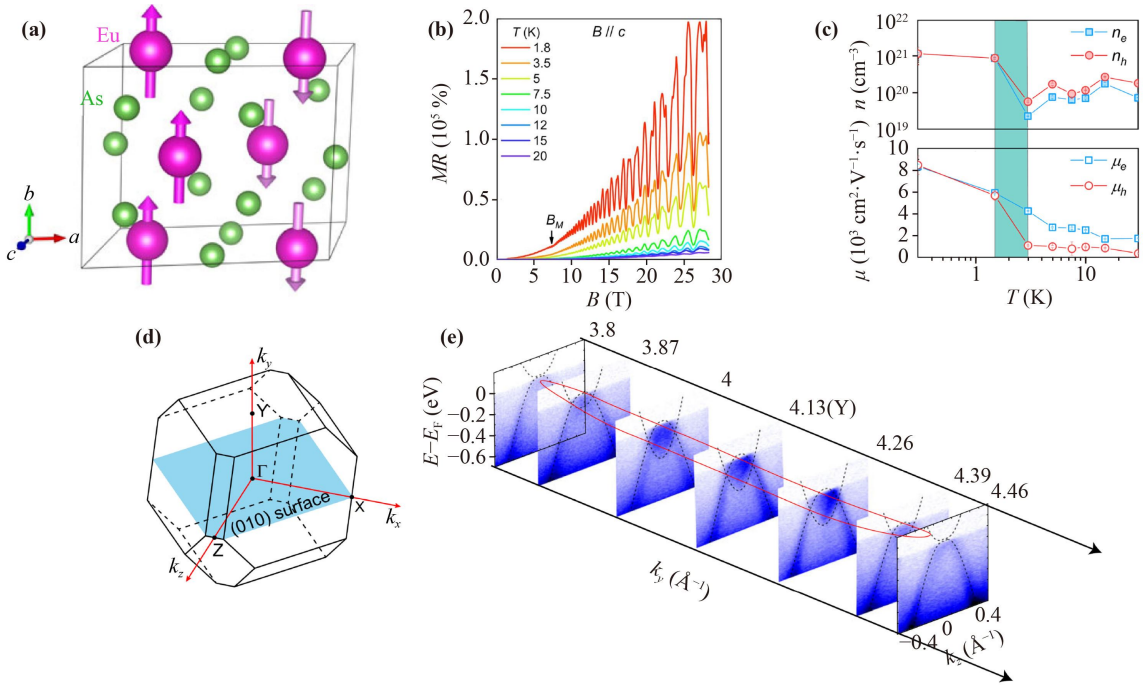

Fig. 15 **(a)** Crystal structure of EuAs$_3$ [268]. **(b)** Magnetoresistance measurements [268]. **(c)** Carrier concentration and mobility [268]. **(d)** The Brillouin zone of EuAs$_3$, with high-symmetry points and (010) surface labeled [268]. **(e)** The band dispersions along k_y direction probed by different photon energies. The red ellipse illustrates the topological nontrivial nodal loop schematically [268].

Eu are oriented along with b axis [268]. The specific heat, electrical conductivity, susceptibility measurements [269], neutron diffraction [270], X-ray scattering technique [271, 272] and μSR [273] studies showed that $EuAs_3$ orders in an incommensurate AFM state at $T_N = 11$ K, and goes through an incommensurate-commensurate lock-in phase transition at $T_L = 10.3$ K, reaching a collinear AFM ground state. Electrical transport studies showed an extremely anisotropic magnetoresistance related to the magnetic configuration [274].

Recently, the magnetism-induced topology of $EuAs_3$ has been demonstrated and the origin of extremely anisotropic magnetoresistance has been discussed [268]. An unsaturated extremely anisotropic magnetoresistance of $2 \times 10^5\%$ at 1.8 K and 28.3 T has been observed, as shown in Fig. 15(b). Meanwhile, through the DFT calculations and transport measurements, it is demonstrated that $EuAs_3$ is a magnetic topological massive Dirac metal at AFM ground state. ARPES results probed by different photon energies verify that $EuAs_3$ is a topological nodal semimetal in PM state [Figs. 15(d, e)], this is related to the extremely anisotropic magnetoresistance. For 3 K $\leq T \leq$ 30 K, the concentration of hole carriers is larger than that of electron carriers. Upon decreasing the temperature $T <$ 3 K the concentration of electron carriers is suddenly enhanced, accompanied by a sharp increase in the mobility of hole carriers, indicating a possible Lifshitz transition [Fig. 15(c)].

5 Perspective

In this review, we have gone through several intrinsic magnetic topological states of matter by introducing their representing materials. The interaction between magnetic order and band topology in these materials brings forth characteristic band features such as Dirac gap, Weyl point, Fermi arc, hinge/corner state and so on, produces large Berry curvature and enables novel topological transport responses including quantum anomalous Hall effect, intrinsic anomalous Hall effect, anomalous Nernst effect, negative magnetoresistance as the signature of chiral anomaly and so on. Intrinsic magnetic topological insulators are of fundamental and practical importance because of the potential for the development of dissipationless spintronics, information storage and quantum computation. However, so far only $Mn(Bi,Sb)_2Te_4 \cdot ((Bi,Sb)_2Te_3)_n$ family is firmly verified as intrinsic magnetic topological insulator. For this family of materials, the lack of sizable magnetic gap hinders the realization of quantum anomalous Hall effect at the expected temperature. It is thus highly desired to search for new material systems hosting such topological state. Instead of incorporating magnetism into established topological systems like the way how $Mn(Bi,Sb)_2Te_4 \cdot ((Bi,Sb)_2Te_3)_n$ and magnetically doped $Bi_2(Se,Te)_3$ families are realized, we envision that looking for band topology based on known ferromagnets or antiferromagnets will be more efficient to realize intrinsic magnetic topological insulator. Recent high-throughput calculations and magnetic space group analyses [275–280] have predicted a large number of new magnetic topological materials which provide guidance for experiment.

While we are concentrating on the interplay between magnetism and band topology in these quantum states of matter, it is well known that magnets host many ordered phases such as spin density wave, charge density wave, superconductivity, nematicity and so on. The interplay between band topology and these orders could generate exotic states such as axionic charge-density wave [281], chiral Majorana fermions [282] and the unknown which deserved future theoretical and experimental investigation. Furthermore, besides ferromagnetism and antiferromagnetism, recently a third basic magnetic phase dubbed altermagnetism [282–284] has been developed to describe some supposed antiferromagnets with mysterious behaviors such as anomalous Hall effect [285–287], spin polarized bands [288] and spin splitting torque [289–292]. Novel topological states of matter based on altermagnets remains to be explored.

Acknowledgements This work was supported by the National Key R&D Program of China (Grant Nos. 2022YFA1403700 and 2020YFA0308900), the National Natural Science Foundation of China (NSFC) (Grant Nos. 12074163, 12074161, and 11504159), NSFC Guangdong (No. 2016A030313650), Guangdong Basic and Applied Basic Research Foundation (Grant Nos. 2022B1515020046, 2022B1515130005 and 2021B1515130007), the Guangdong Innovative and Entrepreneurial Research Team Program (Grant Nos. 2019ZT08C044 and 2016ZT06D348), Shenzhen Science and Technology Program (Grant No. KQTD20190929173815000). C.C. acknowledges the assistance of SUSTech Core Research Facilities. C. L. acknowledges additional support from the Highlight Project (No. PHYS-HL-2020-1) of the College of Science, SUSTech.

References

1. C. L. Kane and E. J. Mele, Z_2 topological order and the quantum spin Hall effect, *Phys. Rev. Lett.* 95(14), 146802 (2005)
2. L. Fu and C. L. Kane, Topological insulators with inversion symmetry, *Phys. Rev. B* 76(4), 045302 (2007)
3. L. Fu, C. L. Kane, and E. J. Mele, Topological insulators in three dimensions, *Phys. Rev. Lett.* 98, 106803 (2007)
4. J. E. Moore and L. Balents, Topological invariants of time-reversal-invariant band structures, *Phys. Rev. B* 75(12), 121306 (2007)
5. H. J. Zhang, C. X. Liu, X. L. Qi, X. Dai, Z. Fang, and S. C. Zhang, Topological insulators in Bi_2Se_3, Bi_2Te_3 and Sb_2Te_3 with a single Dirac cone on the surface, *Nat. Phys.* 5(6), 438 (2009)

6. B. A. Bernevig, T. L. Hughes, and S. C. Zhang, Quantum spin Hall effect and topological phase transition in HgTe quantum wells, *Science* 314(5806), 1757 (2006)
7. M. König, S. Wiedmann, C. Brune, A. Roth, H. Buhmann, L. W. Molenkamp, X. L. Qi, and S. C. Zhang, Quantum spin hall insulator state in HgTe quantum wells, *Science* 318(5851), 766 (2007)
8. D. Hsieh, D. Qian, L. Wray, Y. Xia, Y. S. Hor, R. J. Cava, and M. Z. Hasan, A topological Dirac insulator in a quantum spin Hall phase, *Nature* 452(7190), 970 (2008)
9. Y. L. Chen, J. G. Analytis, J. H. Chu, Z. K. Liu, S. K. Mo, X. L. Qi, H. J. Zhang, D. H. Lu, X. Dai, Z. Fang, S. C. Zhang, I. R. Fisher, Z. Hussain, and Z. X. Shen, Experimental realization of a three-dimensional topological insulator, Bi_2Te_3, *Science* 325(5937), 178 (2009)
10. D. Hsieh, Y. Xia, D. Qian, L. Wray, J. H. Dil, F. Meier, J. Osterwalder, L. Patthey, J. G. Checkelsky, N. P. Ong, A. V. Fedorov, H. Lin, A. Bansil, D. Grauer, Y. S. Hor, R. J. Cava, and M. Z. Hasan, A tunable topological insulator in the spin helical Dirac transport regime, *Nature* 460(7259), 1101 (2009)
11. Y. Xia, D. Qian, D. Hsieh, L. Wray, A. Pal, H. Lin, A. Bansil, D. Grauer, Y. S. Hor, R. J. Cava, and M. Z. Hasan, Observation of a large-gap topological-insulator class with a single Dirac cone on the surface, *Nat. Phys.* 5(6), 398 (2009)
12. T. Valla, Z. H. Pan, D. Gardner, Y. S. Lee, and S. Chu, Photoemission spectroscopy of magnetic and nonmagnetic impurities on the surface of the Bi_2Se_3 topological insulator, *Phys. Rev. Lett.* 108(11), 117601 (2012)
13. C. Chen, S. He, H. Weng, W. Zhang, L. Zhao, H. Liu, X. Jia, D. Mou, S. Liu, J. He, Y. Peng, Y. Feng, Z. Xie, G. Liu, X. Dong, J. Zhang, X. Wang, Q. Peng, Z. Wang, S. Zhang, F. Yang, C. Chen, Z. Xu, X. Dai, Z. Fang, and X. J. Zhou, Robustness of topological order and formation of quantum well states in topological insulators exposed to ambient environment, *Proc. Natl. Acad. Sci. USA* 109(10), 3694 (2012)
14. L. A. Wray, S. Y. Xu, Y. Xia, D. Hsieh, A. V. Fedorov, Y. S. Hor, R. J. Cava, A. Bansil, H. Lin, and M. Z. Hasan, A topological insulator surface under strong Coulomb, magnetic and disorder perturbations, *Nat. Phys.* 7, 32 (2011)
15. C. Z. Chang, J. Zhang, X. Feng, J. Shen, Z. Zhang, M. Guo, K. Li, Y. Ou, P. Wei, L. L. Wang, Z. Q. Ji, Y. Feng, S. Ji, X. Chen, J. Jia, X. Dai, Z. Fang, S. C. Zhang, K. He, Y. Wang, L. Lu, X. C. Ma, and Q. K. Xue, Experimental observation of the quantum anomalous Hall effect in a magnetic topological insulator, *Science* 340(6129), 167 (2013)
16. R. Yu, W. Zhang, H. J. Zhang, S. C. Zhang, X. Dai, and Z. Fang, Quantized anomalous Hall effect in magnetic topological insulators, *Science* 329(5987), 61 (2010)
17. N. P. Armitage, E. J. Mele, and A. Vishwanath, Weyl and Dirac semimetals in three-dimensional solids, *Rev. Mod. Phys.* 90(1), 015001 (2018)
18. A. A. Burkov and L. Balents, Weyl semimetal in a topological insulator multilayer, *Phys. Rev. Lett.* 107(12), 127205 (2011)
19. A. A. Burkov, M. D. Hook, and L. Balents, Topological nodal semimetals, *Phys. Rev. B* 84(23), 235126 (2011)
20. X. G. Wan, A. M. Turner, A. Vishwanath, and S. Y. Savrasov, Topological semimetal and Fermi-arc surface states in the electronic structure of pyrochlore iridates, *Phys. Rev. B* 83(20), 205101 (2011)
21. Z. Wang, Y. Sun, X. Q. Chen, C. Franchini, G. Xu, H. Weng, X. Dai, and Z. Fang, Dirac semimetal and topological phase transitions in A_3Bi (A=Na, K, Rb), *Phys. Rev. B* 85(19), 195320 (2012)
22. S. M. Young, S. Zaheer, J. C. Y. Teo, C. L. Kane, E. J. Mele, and A. M. Rappe, Dirac semimetal in three dimensions, *Phys. Rev. Lett.* 108(14), 140405 (2012)
23. Z. J. Wang, H. M. Weng, Q. S. Wu, X. Dai, and Z. Fang, Three-dimensional Dirac semimetal and quantum transport in Cd_3As_2, *Phys. Rev. B* 88(12), 125427 (2013)
24. W. Ning and Z. Mao, Recent advancements in the study of intrinsic magnetic topological insulators and magnetic Weyl semimetals, *APL Mater.* 8(9), 090701 (2020)
25. M. Z. Hasan, G. Chang, I. Belopolski, G. Bian, S. Y. Xu, and J. X. Yin, Weyl, Dirac and high-fold chiral fermions in topological quantum matter, *Nat. Rev. Mater.* 6(9), 784 (2021)
26. B. A. Bernevig, C. Felser, and H. Beidenkopf, Progress and prospects in magnetic topological materials, *Nature* 603(7899), 41 (2022)
27. F. Tang, H. C. Po, A. Vishwanath, and X. Wan, Comprehensive search for topological materials using symmetry indicators, *Nature* 566(7745), 486 (2019)
28. M. G. Vergniory, L. Elcoro, C. Felser, N. Regnault, B. A. Bernevig, and Z. Wang, A complete catalogue of high-quality topological materials, *Nature* 566(7745), 480 (2019)
29. T. Zhang, Y. Jiang, Z. Song, H. Huang, Y. He, Z. Fang, H. Weng, and C. Fang, Catalogue of topological electronic materials, *Nature* 566(7745), 475 (2019)
30. C. Liu and X. R. Liu, Angle resolved photoemission spectroscopy studies on three dimensional strong topological insulators and magnetic topological insulators, *Acta Phys. Sin.* 68(22), 227901 (2019)
31. Y. Ando, Topological insulator materials, *J. Phys. Soc. Jpn.* 82(10), 102001 (2013)
32. J. A. Sobota, Y. He, and Z. X. Shen, Angle-resolved photoemission studies of quantum materials, *Rev. Mod. Phys.* 93(2), 025006 (2021)
33. Y. Wang, On the topological surface states of the intrinsic magnetic topological insulator Mn–Bi–Te family, arXiv: 2211.04017 (2022)
34. Y. Zhao and Q. Liu, Routes to realize the axion-insulator phase in $MnBi_2Te_4(Bi_2Te_3)_n$ family, *Appl. Phys. Lett.* 119(6), 060502 (2021)
35. P. Wang, J. Ge, J. Li, Y. Liu, Y. Xu, and J. Wang, Intrinsic magnetic topological insulators, *Innovation* 2(2), 100098 (2021)
36. Y. Li and Y. Xu, First-principles discovery of novel quantum physics and materials: From theory to experiment, *Comput. Mater. Sci.* 190, 110262 (2021)
37. C. Y. Chen, Surface state energy gap of magnetic

origin and "semi magnetic topological insulator", *Physics* 50, 267 (2021) (in Chinese)
38. K. He, $MnBi_2Te_4$-family intrinsic magnetic topological materials, *npj Quantum Mater.* 5, 90 (2020)
39. G. H. Zhan, H. Q Wang, and H. J. Zhang, Antiferromagnetic topological insulators and axion insulators — $MnBi_2Te_4$ family magnetic systems, *Physics* 49(12), 817 (2020)
40. T. Kida, L. A. Fenner, A. A. Dee, I. Terasaki, M. Hagiwara, and A. S. Wills, The giant anomalous Hall effect in the ferromagnet Fe_3Sn_2 — a frustrated Kagomé metal, *J. Phys.: Condens. Matter* 23(11), 112205 (2011)
41. F. D. M. Haldane, Model for a quantum Hall effect without Landau levels: Condensed-matter realization of the "parity anomaly", *Phys. Rev. Lett.* 61(18), 2015 (1988)
42. P. Y. Chang, O. Erten, and P. Coleman, Möbius Kondo insulators, *Nat. Phys.* 13(8), 794 (2017)
43. K. Shiozaki, M. Sato, and K. Gomi, Z_2 topology in nonsymmorphic crystalline insulators: Möbius twist in surface states, *Phys. Rev. B* 91(15), 155120 (2015)
44. R. X. Zhang, F. Wu, and S. Das Sarma, Mobius insulator and higher-order topology in $MnBi_{2n}Te_{3n+1}$, *Phys. Rev. Lett.* 124(13), 136407 (2020)
45. C. Liu, Y. Wang, H. Li, Y. Wu, Y. Li, J. Li, K. He, Y. Xu, J. Zhang, and Y. Wang, Robust axion insulator and Chern insulator phases in a two-dimensional antiferromagnetic topological insulator, *Nat. Mater.* 19(5), 522 (2020)
46. C. Z. Chang, J. Zhang, X. Feng, J. Shen, Z. Zhang, M. Guo, K. Li, Y. Ou, P. Wei, L. L. Wang, Z. Q. Ji, Y. Feng, S. Ji, X. Chen, J. Jia, X. Dai, Z. Fang, S. C. Zhang, K. He, Y. Wang, L. Lu, X. C. Ma, and Q. K. Xue, Experimental observation of the quantum anomalous Hall effect in a magnetic topological insulator, *Science* 340(6129), 167 (2013)
47. L. Wu, M. Salehi, N. Koirala, J. Moon, S. Oh, and N. P. Armitage, Quantized Faraday and Kerr rotation and axion electrodynamics of a 3D topological insulator, *Science* 354(6316), 1124 (2016)
48. E. Liu, Y. Sun, N. Kumar, L. Muechler, A. Sun, L. Jiao, S. Y. Yang, D. Liu, A. Liang, Q. Xu, J. Kroder, V. Süß, H. Borrmann, C. Shekhar, Z. Wang, C. Xi, W. Wang, W. Schnelle, S. Wirth, Y. Chen, S. T. B. Goennenwein, and C. Felser, Giant anomalous Hall effect in a ferromagnetic Kagomé-lattice semimetal, *Nat. Phys.* 14(11), 1125 (2018)
49. C. L. Zhang, S. Y. Xu, I. Belopolski, Z. Yuan, Z. Lin, B. Tong, G. Bian, N. Alidoust, C. C. Lee, S. M. Huang, T. R. Chang, G. Chang, C. H. Hsu, H. T. Jeng, M. Neupane, D. S. Sanchez, H. Zheng, J. Wang, H. Lin, C. Zhang, H. Z. Lu, S. Q. Shen, T. Neupert, M. Zahid Hasan, and S. Jia, Signatures of the Adler–Bell–Jackiw chiral anomaly in a Weyl fermion semimetal, *Nat. Commun.* 7(1), 10735 (2016)
50. S. N. Guin, P. Vir, Y. Zhang, N. Kumar, S. J. Watzman, C. Fu, E. Liu, K. Manna, W. Schnelle, J. Gooth, C. Shekhar, Y. Sun, and C. Felser, Zero-field Nernst effect in a ferromagnetic Kagomé-lattice Weyl-semimetal $Co_3Sn_2S_2$, *Adv. Mater.* 31(25), 1806622 (2019)
51. E. K. Liu and S. Zhang, Topologically enhanced zero-field transverse Nernst thermoelectric effect in magnetic topological semimetals, *Sci. China Phys. Mech. & Astron.* 49(12), 127001 (2019)
52. R. S. K. Mong, A. M. Essin, and J. E. Moore, Antiferromagnetic topological insulators, *Phys. Rev. B* 81(24), 245209 (2010)
53. M. M. Otrokov, T. V. Menshchikova, M. G. Vergniory, I. P. Rusinov, A. Yu Vyazovskaya, Y. M. Koroteev, G. Bihlmayer, A. Ernst, P. M. Echenique, A. Arnau, and E. V. Chulkov, Highly-ordered wide bandgap materials for quantized anomalous Hall and magnetoelectric effects, *2D Mater.* 4, 025082 (2017)
54. M. M. Otrokov, T. V. Menshchikova, I. P. Rusinov, M. G. Vergniory, V. M. Kuznetsov, and E. V. Chulkov, Magnetic extension as an efficient method for realizing the quantum anomalous hall state in topological insulators, *JETP Lett.* 105(5), 297 (2017)
55. Y. Gong, J. Guo, J. Li, K. Zhu, M. Liao, X. Liu, Q. Zhang, L. Gu, L. Tang, X. Feng, D. Zhang, W. Li, C. Song, L. Wang, P. Yu, X. Chen, Y. Wang, H. Yao, W. Duan, Y. Xu, S. C. Zhang, X. Ma, Q. K. Xue, and K. He, Experimental realization of an intrinsic magnetic topological insulator, *Chin. Phys. Lett.* 36(7), 076801 (2019)
56. D. Zhang, M. Shi, T. Zhu, D. Xing, H. Zhang, and J. Wang, Topological axion states in the magnetic insulator $MnBi_2Te_4$ with the quantized magnetoelectric effect, *Phys. Rev. Lett.* 122(20), 206401 (2019)
57. M. M. Otrokov, I. P. Rusinov, M. Blanco-Rey, M. Hoffmann, A. Y. Vyazovskaya, S. V. Eremeev, A. Ernst, P. M. Echenique, A. Arnau, and E. V. Chulkov, Unique thickness-dependent properties of the van der Waals interlayer antiferromagnet $MnBi_2Te_4$ films, *Phys. Rev. Lett.* 122(10), 107202 (2019)
58. J. Li, Y. Li, S. Du, Z. Wang, B. L. Gu, S. C. Zhang, K. He, W. Duan, and Y. Xu, Intrinsic magnetic topological insulators in van der Waals layered $MnBi_2Te_4$-family materials, *Sci. Adv.* 5(6), eaaw5685 (2019)
59. M. M. Otrokov, I. I. Klimovskikh, H. Bentmann, D. Estyunin, A. Zeugner, Z. S. Aliev, S. Gaß, A. U. B. Wolter, A. V. Koroleva, A. M. Shikin, M. Blanco-Rey, M. Hoffmann, I. P. Rusinov, A. Y. Vyazovskaya, S. V. Eremeev, Y. M. Koroteev, V. M. Kuznetsov, F. Freyse, J. Sánchez-Barriga, I. R. Amiraslanov, M. B. Babanly, N. T. Mamedov, N. A. Abdullayev, V. N. Zverev, A. Alfonsov, V. Kataev, B. Büchner, E. F. Schwier, S. Kumar, A. Kimura, L. Petaccia, G. Di Santo, R. C. Vidal, S. Schatz, K. Kißner, M. Ünzelmann, C. H. Min, S. Moser, T. R. F. Peixoto, F. Reinert, A. Ernst, P. M. Echenique, A. Isaeva, and E. V. Chulkov, Prediction and observation of an antiferromagnetic topological insulator, *Nature* 576(7787), 416 (2019)
60. Z. S. Aliev, I. R. Amiraslanov, D. I. Nasonova, A. V. Shevelkov, N. A. Abdullayev, Z. A. Jahangirli, E. N. Orujlu, M. M. Otrokov, N. T. Mamedov, M. B. Babanly, and E. V. Chulkov, Novel ternary layered manganese bismuth tellurides of the $MnTe–Bi_2Te_3$ system: Synthesis and crystal structure, *J. Alloys Compd.* 789, 443 (2019)

61. J. Wu, F. Liu, C. Liu, Y. Wang, C. Li, Y. Lu, S. Matsuishi, and H. Hosono, Toward 2D magnets in the $(MnBi_2Te_4)(Bi_2Te_3)_n$ bulk crystal, *Adv. Mater.* 32(23), e2001815 (2020)
62. D. Souchay, M. Nentwig, D. Günther, S. Keilholz, J. de Boor, A. Zeugner, A. Isaeva, M. Ruck, A. U. B. Wolter, B. Büchner, and O. Oeckler, Layered manganese bismuth tellurides with $GeBi_4Te_7$- and $GeBi_6Te_{10}$-type structures: Towards multifunctional materials, *J. Mater. Chem. C* 7(32), 9939 (2019)
63. D. S. Lee, T. H. Kim, C. H. Park, C. Y. Chung, Y. S. Lim, W. S. Seo, and H. H. Park, Crystal structure, properties and nanostructuring of a new layered chalcogenide semiconductor, Bi_2MnTe_4, *CrystEngComm* 15(27), 5532 (2013)
64. T. Hirahara, S. V. Eremeev, T. Shirasawa, Y. Okuyama, T. Kubo, R. Nakanishi, R. Akiyama, A. Takayama, T. Hajiri, S. I. Ideta, M. Matsunami, K. Sumida, K. Miyamoto, Y. Takagi, K. Tanaka, T. Okuda, T. Yokoyama, S. I. Kimura, S. Hasegawa, and E. V. Chulkov, Large-gap magnetic topological heterostructure formed by subsurface incorporation of a ferromagnetic layer, *Nano Lett.* 17(6), 3493 (2017)
65. J. A. Hagmann, X. Li, S. Chowdhury, S. N. Dong, S. Rouvimov, S. J. Pookpanratana, K. Man Yu, T. A. Orlova, T. B. Bolin, C. U. Segre, D. G. Seiler, C. A. Richter, X. Liu, M. Dobrowolska, and J. K. Furdyna, Molecular beam epitaxy growth and structure of self-assembled Bi_2Se_3/Bi_2MnSe_4 multilayer heterostructures, *New J. Phys.* 19(8), 085002 (2017)
66. L. Ding, C. Hu, F. Ye, E. Feng, N. Ni, and H. Cao, Crystal and magnetic structures of magnetic topological insulators $MnBi_2Te_4$ and $MnBi_4Te_7$, *Phys. Rev. B* 101(2), 020412 (2020)
67. J. Q. Yan, Q. Zhang, T. Heitmann, Z. Huang, K. Y. Chen, J. G. Cheng, W. Wu, D. Vaknin, B. C. Sales, and R. J. McQueeney, Crystal growth and magnetic structure of $MnBi_2Te_4$, *Phys. Rev. Mater.* 3(6), 064202 (2019)
68. M. Z. Shi, B. Lei, C. S. Zhu, D. H. Ma, J. H. Cui, Z. L. Sun, J. J. Ying, and X. H. Chen, Magnetic and transport properties in the magnetic topological insulators $MnBi_2Te_4(Bi_2Te_3)_n$ (n=1, 2), *Phys. Rev. B* 100(15), 155144 (2019)
69. Y. J. Hao, P. Liu, Y. Feng, X. M. Ma, E. F. Schwier, M. Arita, S. Kumar, C. Hu, R. Lu, M. Zeng, Y. Wang, Z. Hao, H. Y. Sun, K. Zhang, J. Mei, N. Ni, L. Wu, K. Shimada, C. Chen, Q. Liu, and C. Liu, Gapless surface Dirac cone in antiferromagnetic topological insulator $MnBi_2Te_4$, *Phys. Rev. X* 9, 041038 (2019)
70. C. Hu, K. N. Gordon, P. Liu, J. Liu, X. Zhou, P. Hao, D. Narayan, E. Emmanouilidou, H. Sun, Y. Liu, H. Brawer, A. P. Ramirez, L. Ding, H. Cao, Q. Liu, D. Dessau, and N. Ni, A van der Waals antiferromagnetic topological insulator with weak interlayer magnetic coupling, *Nat. Commun.* 11(1), 97 (2020)
71. X. M. Ma, Z. Chen, E. F. Schwier, Y. Zhang, Y. J. Hao, S. Kumar, R. Lu, J. Shao, Y. Jin, M. Zeng, X. R. Liu, Z. Hao, K. Zhang, W. Mansuer, C. Song, Y. Wang, B. Zhao, C. Liu, K. Deng, J. Mei, K. Shimada, Y. Zhao, X. Zhou, B. Shen, W. Huang, C. Liu, H. Xu, and C. Chen, Hybridization-induced gapped and gapless states on the surface of magnetic topological insulators, *Phys. Rev. B* 102(24), 245136 (2020)
72. R. Lu, H. Sun, S. Kumar, Y. Wang, M. Gu, M. Zeng, Y. J. Hao, J. Li, J. Shao, X. M. Ma, Z. Hao, K. Zhang, W. Mansuer, J. Mei, Y. Zhao, C. Liu, K. Deng, W. Huang, B. Shen, K. Shimada, E. F. Schwier, C. Liu, Q. Liu, and C. Chen, Half-magnetic topological insulator with magnetization-induced Dirac gap at a selected surface, *Phys. Rev. X* 11(1), 011039 (2021)
73. Y. J. Chen, L. X. Xu, J. H. Li, Y. W. Li, H. Y. Wang, C. F. Zhang, H. Li, Y. Wu, A. J. Liang, C. Chen, S. W. Jung, C. Cacho, Y. H. Mao, S. Liu, M. X. Wang, Y. F. Guo, Y. Xu, Z. K. Liu, L. X. Yang, and Y. L. Chen, Topological electronic structure and its temperature evolution in antiferromagnetic topological insulator $MnBi_2Te_4$, *Phys. Rev. X* 9(4), 041040 (2019)
74. H. Li, S. Y. Gao, S. F. Duan, Y. F. Xu, K. J. Zhu, S. J. Tian, J. C. Gao, W. H. Fan, Z. C. Rao, J. R. Huang, J. J. Li, D. Y. Yan, Z. T. Liu, W. L. Liu, Y. B. Huang, Y. L. Li, Y. Liu, G. B. Zhang, P. Zhang, T. Kondo, S. Shin, H. C. Lei, Y. G. Shi, W. T. Zhang, H. M. Weng, T. Qian, and H. Ding, Dirac surface states in intrinsic magnetic topological insulators $EuSn_2As_2$ and $MnBi_{2n}Te_{3n+1}$, *Phys. Rev. X* 9(4), 041039 (2019)
75. A. Liang, C. Chen, H. Zheng, W. Xia, K. Huang, L. Wei, H. Yang, Y. Chen, X. Zhang, X. Xu, M. Wang, Y. Guo, L. Yang, Z. Liu, and Y. Chen, Approaching a minimal topological electronic structure in antiferromagnetic topological insulator $MnBi_2Te_4$ via surface modification, *Nano Lett.* 22(11), 4307 (2022)
76. R. Xu, Y. Bai, J. Zhou, J. Li, X. Gu, N. Qin, Z. Yin, X. Du, Q. Zhang, W. Zhao, Y. Li, Y. Wu, C. Ding, L. Wang, A. Liang, Z. Liu, Y. Xu, X. Feng, K. He, Y. Chen, and L. Yang, Evolution of the electronic structure of ultrathin $MnBi_2Te_4$ films, *Nano Lett.* 22(15), 6320 (2022)
77. R. C. Vidal, H. Bentmann, T. R. F. Peixoto, A. Zeugner, S. Moser, C. H. Min, S. Schatz, K. Kißner, M. Ünzelmann, C. I. Fornari, H. B. Vasili, M. Valvidares, K. Sakamoto, D. Mondal, J. Fujii, I. Vobornik, S. Jung, C. Cacho, T. K. Kim, R. J. Koch, C. Jozwiak, A. Bostwick, J. D. Denlinger, E. Rotenberg, J. Buck, M. Hoesch, F. Diekmann, S. Rohlf, M. Kalläne, K. Rossnagel, M. M. Otrokov, E. V. Chulkov, M. Ruck, A. Isaeva, and F. Reinert, Surface states and Rashba-type spin polarization in antiferromagnetic $MnBi_2Te_4$ (0001), *Phys. Rev. B* 100(12), 121104 (2019)
78. S. H. Lee, Y. Zhu, Y. Wang, L. Miao, T. Pillsbury, H. Yi, S. Kempinger, J. Hu, C. A. Heikes, P. Quarterman, W. Ratcliff, J. A. Borchers, H. Zhang, X. Ke, D. Graf, N. Alem, C. Z. Chang, N. Samarth, and Z. Mao, Spin scattering and noncollinear spin structure-induced intrinsic anomalous Hall effect in antiferromagnetic topological insulator $MnBi_2Te_4$, *Phys. Rev. Res.* 1(1), 012011 (2019)
79. Y. Hu, L. Xu, M. Shi, A. Luo, S. Peng, Z. Y. Wang, J. J. Ying, T. Wu, Z. K. Liu, C. F. Zhang, Y. L. Chen, G. Xu, X. H. Chen, and J. F. He, Universal gapless Dirac cone and tunable topological states in $(MnBi_2Te_4)_m(Bi_2Te_3)_n$ heterostructures, *Phys. Rev. B* 101, 161113(R) (2020)
80. D. Nevola, H. X. Li, J. Q. Yan, R. G. Moore, H. N.

Lee, H. Miao, and P. D. Johnson, Coexistence of surface ferromagnetism and a gapless topological state in $MnBi_2Te_4$, *Phys. Rev. Lett.* 125(11), 117205 (2020)

81. A. M. Shikin, D. A. Estyunin, I. I. Klimovskikh, S. O. Filnov, E. F. Schwier, S. Kumar, K. Miyamoto, T. Okuda, A. Kimura, K. Kuroda, K. Yaji, S. Shin, Y. Takeda, Y. Saitoh, Z. S. Aliev, N. T. Mamedov, I. R. Amiraslanov, M. B. Babanly, M. M. Otrokov, S. V. Eremeev, and E. V. Chulkov, Nature of the Dirac gap modulation and surface magnetic interaction in axion antiferromagnetic topological insulator $MnBi_2Te_4$, *Sci. Rep.* 10(1), 13226 (2020)
82. P. Swatek, Y. Wu, L. L. Wang, K. Lee, B. Schrunk, J. Yan, and A. Kaminski, Gapless Dirac surface states in the antiferromagnetic topological insulator $MnBi_2Te_4$, *Phys. Rev. B* 101(16), 161109 (2020)
83. A. M. Shikin, D. A. Estyunin, N. L. Zaitsev, D. Glazkova, I. I. Klimovskikh, S. O. Filnov, A. G. Rybkin, E. F. Schwier, S. Kumar, A. Kimura, N. Mamedov, Z. Aliev, M. B. Babanly, K. Kokh, O. E. Tereshchenko, M. M. Otrokov, E. V. Chulkov, K. A. Zvezdin, and A. K. Zvezdin, Sample-dependent Dirac-point gap in $MnBi_2Te_4$ and its response to applied surface charge: A combined photoemission and *ab initio* study, *Phys. Rev. B* 104(11), 115168 (2021)
84. R. C. Vidal, H. Bentmann, J. I. Facio, T. Heider, P. Kagerer, C. I. Fornari, T. R. F. Peixoto, T. Figgemeier, S. Jung, C. Cacho, B. Buchner, J. van den Brink, C. M. Schneider, L. Plucinski, E. F. Schwier, K. Shimada, M. Richter, A. Isaeva, and F. Reinert, Orbital complexity in intrinsic magnetic topological insulators $MnBi_4Te_7$ and $MnBi_6Te_{10}$, *Phys. Rev. Lett.* 126(17), 176403 (2021)
85. X. Wu, J. Li, X. M. Ma, Y. Zhang, Y. Liu, C. S. Zhou, J. Shao, Q. Wang, Y. J. Hao, Y. Feng, E. F. Schwier, S. Kumar, H. Sun, P. Liu, K. Shimada, K. Miyamoto, T. Okuda, K. Wang, M. Xie, C. Chen, Q. Liu, C. Liu, and Y. Zhao, Distinct topological surface states on the two terminations of $MnBi_4Te_7$, *Phys. Rev. X* 10(3), 031013 (2020)
86. S. Tian, S. Gao, S. Nie, Y. Qian, C. Gong, Y. Fu, H. Li, W. Fan, P. Zhang, T. Kondo, S. Shin, J. Adell, H. Fedderwitz, H. Ding, Z. Wang, T. Qian, and H. Lei, Magnetic topological insulator $MnBi_6Te_{10}$ with a zero-field ferromagnetic state and gapped Dirac surface states, *Phys. Rev. B* 102(3), 035144 (2020)
87. I. I. Klimovskikh, M. M. Otrokov, D. Estyunin, S. V. Eremeev, S. O. Filnov, A. Koroleva, E. Shevchenko, V. Voroshnin, A. G. Rybkin, I. P. Rusinov, M. Blanco-Rey, M. Hoffmann, Z. S. Aliev, M. B. Babanly, I. R. Amiraslanov, N. A. Abdullayev, V. N. Zverev, A. Kimura, O. E. Tereshchenko, K. A. Kokh, L. Petaccia, G. Di Santo, A. Ernst, P. M. Echenique, N. T. Mamedov, A. M. Shikin, and E. V. Chulkov, Tunable 3D/2D magnetism in the $(MnBi_2Te_4)(Bi_2Te_3)_m$ topological insulators family, *npj Quantum Mater.* 5, 54 (2020)
88. N. H. Jo, L. L. Wang, R. J. Slager, J. Yan, Y. Wu, K. Lee, B. Schrunk, A. Vishwanath, and A. Kaminski, Intrinsic axion insulating behavior in antiferromagnetic $MnBi_6Te_{10}$, *Phys. Rev. B* 102(4), 045130 (2020)
89. C. Hu, L. Ding, K. N. Gordon, B. Ghosh, H. J. Tien, H. Li, A. G. Linn, S. W. Lien, C. Y. Huang, S. Mackey, J. Liu, P. V. S. Reddy, B. Singh, A. Agarwal, A. Bansil, M. Song, D. Li, S. Y. Xu, H. Lin, H. Cao, T. R. Chang, D. Dessau, and N. Ni, Realization of an intrinsic ferromagnetic topological state in $MnBi_8Te_{13}$, *Sci. Adv.* 6(30), eaba4275 (2020)
90. T. Hirahara, M. M. Otrokov, T. T. Sasaki, K. Sumida, Y. Tomohiro, S. Kusaka, Y. Okuyama, S. Ichinokura, M. Kobayashi, Y. Takeda, K. Amemiya, T. Shirasawa, S. Ideta, K. Miyamoto, K. Tanaka, S. Kuroda, T. Okuda, K. Hono, S. V. Eremeev, and E. V. Chulkov, Fabrication of a novel magnetic topological heterostructure and temperature evolution of its massive Dirac cone, *Nat. Commun.* 11(1), 4821 (2020)
91. J. Wu, F. Liu, M. Sasase, K. Ienaga, Y. Obata, R. Yukawa, K. Horiba, H. Kumigashira, S. Okuma, T. Inoshita, and H. Hosono, Natural van der Waals heterostructural single crystals with both magnetic and topological properties, *Sci. Adv.* 5(11), eaax9989 (2019)
92. R. C. Vidal, A. Zeugner, J. I. Facio, R. Ray, M. H. Haghighi, A. U. B. Wolter, L. T. Corredor Bohorquez, F. Caglieris, S. Moser, T. Figgemeier, T. R. F. Peixoto, H. B. Vasili, M. Valvidares, S. Jung, C. Cacho, A. Alfonsov, K. Mehlawat, V. Kataev, C. Hess, M. Richter, B. Büchner, J. van den Brink, M. Ruck, F. Reinert, H. Bentmann, and A. Isaeva, Topological electronic structure and intrinsic magnetization in $MnBi_4Te_7$: A Bi_2Te_3 derivative with a periodic Mn sublattice, *Phys. Rev. X* 9(4), 041065 (2019)
93. Y. Deng, Y. Yu, Z. S. Meng, Z. Guo, Z. Xu, J. Wang, H. C. Xian, and Y. Zhang, Quantum anomalous Hall effect in intrinsic magnetic topological insulator $MnBi_2Te_4$, *Science* 367(6480), 895 (2020)
94. J. Ge, Y. Liu, J. Li, H. Li, T. Luo, Y. Wu, Y. Xu, and J. Wang, High-Chern-number and high-temperature quantum Hall effect without Landau levels, *Natl. Sci. Rev.* 7(8), 1280 (2020)
95. A. Gao, Y. F. Liu, C. Hu, J. X. Qiu, C. Tzschaschel, B. Ghosh, S. C. Ho, D. Berube, R. Chen, H. Sun, Z. Zhang, X. Y. Zhang, Y. X. Wang, N. Wang, Z. Huang, C. Felser, A. Agarwal, T. Ding, H. J. Tien, A. Akey, J. Gardener, B. Singh, K. Watanabe, T. Taniguchi, K. S. Burch, D. C. Bell, B. B. Zhou, W. Gao, H. Z. Lu, A. Bansil, H. Lin, T. R. Chang, L. Fu, Q. Ma, N. Ni, and S. Y. Xu, Layer Hall effect in a 2D topological axion antiferromagnet, *Nature* 595(7868), 521 (2021)
96. S. Li, M. Gong, S. Cheng, H. Jiang, and X. C. Xie, Dissipationless layertronics in axion insulator $MnBi_2Te_4$, arXiv: 2207.09186 (2022)
97. L. Xu, Y. Mao, H. Wang, J. Li, Y. Chen, Y. Xia, Y. Li, D. Pei, J. Zhang, H. Zheng, K. Huang, C. Zhang, S. Cui, A. Liang, W. Xia, H. Su, S. Jung, C. Cacho, M. Wang, G. Li, Y. Xu, Y. Guo, L. Yang, Z. Liu, Y. Chen, and M. Jiang, Persistent surface states with diminishing gap in $MnBi_2Te_4/Bi_2Te_3$ superlattice antiferromagnetic topological insulator, *Sci. Bull. (Beijing)* 65(24), 2086 (2020)
98. S. V. Eremeev, I. P. Rusinov, Y. M. Koroteev, A. Y. Vyazovskaya, M. Hoffmann, P. M. Echenique, A. Ernst, M. M. Otrokov, and E. V. Chulkov, Topological magnetic materials of the $(MnSb_2Te_4)\cdot(Sb_2Te_3)_n$ van der Waals compounds family, *J. Phys. Chem. Lett.* 12(17), 4268 (2021)

99. S. V. Eremeev, M. M. Otrokov, and E. V. Chulkov, Competing rhombohedral and monoclinic crystal structures in $MnPn_2Ch_4$ compounds: An *ab-initio* study, *J. Alloys Compd.* 709, 172 (2017)
100. T. Murakami, Y. Nambu, T. Koretsune, G. Xiangyu, T. Yamamoto, C. M. Brown, and H. Kageyama, Realization of interlayer ferromagnetic interaction in $MnSb_2Te_4$ toward the magnetic Weyl semimetal state, *Phys. Rev. B* 100(19), 195103 (2019)
101. J. Q. Yan, S. Okamoto, M. A. McGuire, A. F. May, R. J. McQueeney, and B. C. Sales, Evolution of structural, magnetic, and transport properties in $MnBi_{2-x}Sb_xTe_4$, *Phys. Rev. B* 100(10), 104409 (2019)
102. L. Chen, D. Wang, C. Shi, C. Jiang, H. Liu, G. Cui, X. Zhang, and X. Li, Electronic structure and magnetism of $MnSb_2Te_4$, *J. Mater. Sci.* 55(29), 14292 (2020)
103. Y. Chen, Y. W. Chuang, S. H. Lee, Y. Zhu, K. Honz, Y. Guan, Y. Wang, K. Wang, Z. Mao, J. Zhu, C. Heikes, P. Quarterman, P. Zajdel, J. A. Borchers, and W. Ratcliff, Ferromagnetism in van der Waals compound $MnSb_{1.8}Bi_{0.2}Te_4$, *Phys. Rev. Mater.* 4(6), 064411 (2020)
104. G. Shi, M. Zhang, D. Yan, H. Feng, M. Yang, Y. Shi, and Y. Li, Anomalous Hall effect in layered ferrimagnet $MnSb_2Te_4$, *Chin. Phys. Lett.* 37(4), 047301 (2020)
105. S. Wimmer, J. Sanchez-Barriga, P. Kuppers, A. Ney, E. Schierle, F. Freyse, O. Caha, J. Michalicka, M. Liebmann, D. Primetzhofer, M. Hoffman, A. Ernst, M. M. Otrokov, G. Bihlmayer, E. Weschke, B. Lake, E. V. Chulkov, M. Morgenstern, G. Bauer, G. Springholz, and O. Rader, Mn-rich $MnSb_2Te_4$: A topological insulator with magnetic gap closing at high Curie temperatures of 45–50 K, *Adv. Mater.* 33(42), 2102935 (2021)
106. Z. Zang, Y. Zhu, M. Xi, S. Tian, T. Wang, P. Gu, Y. Peng, S. Yang, X. Xu, Y. Li, B. Han, L. Liu, Y. Wang, P. Gao, J. Yang, H. Lei, Y. Huang, and Y. Ye, Layer-number-dependent antiferromagnetic and ferromagnetic behavior in $MnSb_2Te_4$, *Phys. Rev. Lett.* 128(1), 017201 (2022)
107. S. Huan, S. Zhang, Z. Jiang, H. Su, H. Wang, X. Zhang, Y. Yang, Z. Liu, X. Wang, N. Yu, Z. Zou, D. Shen, J. Liu, and Y. Guo, Multiple magnetic topological phases in bulk van der Waals crystal $MnSb_4Te_7$, *Phys. Rev. Lett.* 126(24), 246601 (2021)
108. Y. Yin, X. Ma, D. Yan, C. Yi, B. Yue, J. Dai, L. Zhao, X. Yu, Y. Shi, J. T. Wang, and F. Hong, Pressure-driven electronic and structural phase transition in intrinsic magnetic topological insulator $MnSb_2Te_4$, *Phys. Rev. B* 104(17), 174114 (2021)
109. J. Y. Lin, Z. J. Chen, W. Q. Xie, X. B. Yang, and Y. J. Zhao, Toward ferromagnetic semimetal ground state with multiple Weyl nodes in van der Waals crystal $MnSb_4Te_7$, *New J. Phys.* 24(4), 043033 (2022)
110. C. Pei, M. Xi, Q. Wang, W. Shi, J. Wu, L. Gao, Y. Zhao, S. Tian, W. Cao, C. Li, M. Zhang, S. Zhu, Y. Chen, H. Lei, and Y. Qi, Pressure-induced superconductivity in magnetic topological insulator candidate $MnSb_4Te_7$, *Phys. Rev. Mater.* 6(10), L101801 (2022)
111. X. Zhang, Tunable intrinsic ferromagnetic topological phases in bulk van der Waals crystal $MnSb_6Te_{10}$, arXiv: 2111.04973 (2021)
112. X. M. Ma, Y. Zhao, K. Zhang, S. Kumar, R. Lu, J. Li, Q. Yao, J. Shao, F. Hou, X. Wu, M. Zeng, Y. J. Hao, Z. Hao, Y. Wang, X. R. Liu, H. Shen, H. Sun, J. Mei, K. Miyamoto, T. Okuda, M. Arita, E. F. Schwier, K. Shimada, K. Deng, C. Liu, J. Lin, Y. Zhao, C. Chen, Q. Liu, and C. Liu, Realization of a tunable surface Dirac gap in Sb-doped $MnBi_2Te_4$, *Phys. Rev. B* 103(12), L121112 (2021)
113. T. Zhu, A. J. Bishop, T. Zhou, M. Zhu, D. J. O'Hara, A. A. Baker, S. Cheng, R. C. Walko, J. J. Repicky, T. Liu, J. A. Gupta, C. M. Jozwiak, E. Rotenberg, J. Hwang, I. Zutic, and R. K. Kawakami, Synthesis, magnetic properties, and electronic structure of magnetic topological insulator $MnBi_2Se_4$, *Nano Lett.* 21(12), 5083 (2021)
114. M. Q. Arguilla, N. D. Cultrara, Z. J. Baum, S. Jiang, R. D. Ross, and J. E. Goldberger, $EuSn_2As_2$: an exfoliatable magnetic layered Zintl–Klemm phase, *Inorg. Chem. Front.* 4(2), 378 (2017)
115. F. Kabir, Observation of multiple Dirac states in a magnetic topological material $EuMg_2Bi_2$, arXiv: 1912.08645 (2019)
116. S. Regmi, M. M. Hosen, B. Ghosh, B. Singh, G. Dhakal, C. Sims, B. Wang, F. Kabir, K. Dimitri, Y. Liu, A. Agarwal, H. Lin, D. Kaczorowski, A. Bansil, and M. Neupane, Temperature-dependent electronic structure in a higher-order topological insulator candidate $EuIn_2As_2$, *Phys. Rev. B* 102(16), 165153 (2020)
117. M. Marshall, I. Pletikosić, M. Yahyavi, H. J. Tien, T. R. Chang, H. Cao, and W. Xie, Magnetic and electronic structures of antiferromagnetic topological material candidate $EuMg_2Bi_2$, *J. Appl. Phys.* 129(3), 035106 (2021)
118. Y. Zhang, K. Deng, X. Zhang, M. Wang, Y. Wang, C. Liu, J. W. Mei, S. Kumar, E. F. Schwier, K. Shimada, C. Chen, and B. Shen, In-plane antiferromagnetic moments and magnetic polaron in the axion topological insulator candidate $EuIn_2As_2$, *Phys. Rev. B* 101(20), 205126 (2020)
119. L. Zhao, C. Yi, C. T. Wang, Z. Chi, Y. Yin, X. Ma, J. Dai, P. Yang, B. Yue, J. Cheng, F. Hong, J. T. Wang, Y. Han, Y. Shi, and X. Yu, Monoclinic $EuSn_2As_2$: A novel high-pressure network structure, *Phys. Rev. Lett.* 126(15), 155701 (2021)
120. S. X. M. Riberolles, T. V. Trevisan, B. Kuthanazhi, T. W. Heitmann, F. Ye, D. C. Johnston, S. L. Bud'ko, D. H. Ryan, P. C. Canfield, A. Kreyssig, A. Vishwanath, R. J. McQueeney, L. Wang, P. P. Orth, and B. G. Ueland, Magnetic crystalline-symmetry-protected axion electrodynamics and field-tunable unpinned Dirac cones in $EuIn_2As_2$, *Nat. Commun.* 12(1), 999 (2021)
121. H. C. Chen, Z. F. Lou, Y. X. Zhou, Q. Chen, B. J. Xu, S. J. Chen, J. H. Du, J. H. Yang, H. D. Wang, and M. H. Fang, Negative magnetoresistance in antiferromagnetic topological insulator $EuSn_2As_2$, *Chin. Phys. Lett.* 37(4), 047201 (2020)
122. H. Li, W. Gao, Z. Chen, W. Chu, Y. Nie, S. Ma, Y. Han, M. Wu, T. Li, Q. Niu, W. Ning, X. Zhu, and M. Tian, Magnetic properties of the layered magnetic topological insulator $EuSn_2As_2$, *Phys. Rev. B* 104(5), 054435 (2021)

123. H. Sun, C. Chen, Y. Hou, W. Wang, Y. Gong, M. Huo, L. Li, J. Yu, W. Cai, N. Liu, R. Wu, D. X. Yao, and M. Wang, Magnetism variation of the compressed antiferromagnetic topological insulator $EuSn_2As_2$, *Sci. China Phys. Mech. Astron.* 64(11), 118211 (2021)
124. A. M. Goforth, P. Klavins, J. C. Fettinger, and S. M. Kauzlarich, Magnetic properties and negative colossal magnetoresistance of the rare earth Zintl phase $EuIn_2As_2$, *Inorg. Chem.* 47(23), 11048 (2008)
125. T. Tolinski and D. Kaczorowski, Magnetic properties of the putative higher-order topological insulator $EuIn_2As_2$, *SciPost Physics Proceedings*, doi: 10.21468/SciPostPhysProc (2022)
126. Y. Xu, Z. Song, Z. Wang, H. Weng, and X. Dai, Higher-order topology of the axion insulator $EuIn_2As_2$, *Phys. Rev. Lett.* 122(25), 256402 (2019)
127. M. Gong, D. Sar, J. Friedman, D. Kaczorowski, S. Abdel Razek, W. C. Lee, and P. Aynajian, Surface state evolution induced by magnetic order in axion insulator candidate $EuIn_2As_2$, *Phys. Rev. B* 106(12), 125156 (2022)
128. P. Rosa, Y. Xu, M. Rahn, J. Souza, S. Kushwaha, L. Veiga, A. Bombardi, S. Thomas, M. Janoschek, E. Bauer, M. Chan, Z. Wang, J. Thompson, N. Harrison, P. Pagliuso, A. Bernevig, and F. Ronning, Colossal magnetoresistance in a nonsymmorphic antiferromagnetic insulator, *npj Quantum Mater.* 5, 52 (2020)
129. N. Varnava, T. Berry, T. M. McQueen, and D. Vanderbilt, Engineering magnetic topological insulators in $Eu_5M_2X_6$ Zintl compounds, *Phys. Rev. B* 105(23), 235128 (2022)
130. H. Wang, N. Mao, X. Hu, Y. Dai, B. Huang, and C. Niu, A magnetic topological insulator in two-dimensional $EuCd_2Bi_2$: giant gap with robust topology against magnetic transitions, *Mater. Horiz.* 8(3), 956 (2021)
131. J. Liu, S. Meng, and J. T. Sun, Spin-orientation-dependent topological states in two-dimensional antiferromagnetic $NiTl_2S_4$ monolayers, *Nano Lett.* 19(5), 3321 (2019)
132. P. Tang, Q. Zhou, G. Xu, and S. C. Zhang, Dirac fermions in an antiferromagnetic semimetal, *Nat. Phys.* 12(12), 1100 (2016)
133. J. Wang, Antiferromagnetic Dirac semimetals in two dimensions, *Phys. Rev. B* 95(11), 115138 (2017)
134. S. M. Young and B. J. Wieder, Filling-enforced magnetic Dirac semimetals in two dimensions, *Phys. Rev. Lett.* 118(18), 186401 (2017)
135. S. Li, Y. Liu, Z. M. Yu, Y. Jiao, S. Guan, X. L. Sheng, Y. Yao, and S. A. Yang, Two-dimensional antiferromagnetic Dirac fermions in monolayer $TaCoTe_2$, *Phys. Rev. B* 100(20), 205102 (2019)
136. N. Morali, R. Batabyal, P. K. Nag, E. Liu, Q. Xu, Y. Sun, B. Yan, C. Felser, N. Avraham, and H. Beidenkopf, Fermi-arc diversity on surface terminations of the magnetic Weyl semimetal $Co_3Sn_2S_2$, *Science* 365(6459), 1286 (2019)
137. D. F. Liu, A. J. Liang, E. K. Liu, Q. N. Xu, Y. W. Li, C. Chen, D. Pei, W. J. Shi, S. K. Mo, P. Dudin, T. Kim, C. Cacho, G. Li, Y. Sun, L. X. Yang, Z. K. Liu, S. S. P. Parkin, C. Felser, and Y. L. Chen, Magnetic Weyl semimetal phase in a Kagomé crystal, *Science* 365(6459), 1282 (2019)
138. K. Kuroda, T. Tomita, M. T. Suzuki, C. Bareille, A. A. Nugroho, P. Goswami, M. Ochi, M. Ikhlas, M. Nakayama, S. Akebi, R. Noguchi, R. Ishii, N. Inami, K. Ono, H. Kumigashira, A. Varykhalov, T. Muro, T. Koretsune, R. Arita, S. Shin, T. Kondo, and S. Nakatsuji, Evidence for magnetic Weyl fermions in a correlated metal, *Nat. Mater.* 16(11), 1090 (2017)
139. A. K. Nayak, J. E. Fischer, Y. Sun, B. Yan, J. Karel, A. C. Komarek, C. Shekhar, N. Kumar, W. Schnelle, J. Kübler, C. Felser, and S. S. P. Parkin, Large anomalous Hall effect driven by a nonvanishing Berry curvature in the noncolinear antiferromagnet Mn_3Ge, *Sci. Adv.* 2(4), e1501870 (2016)
140. S. Nakatsuji, N. Kiyohara, and T. Higo, Large anomalous Hall effect in a non-collinear antiferromagnet at room temperature, *Nature* 527(7577), 212 (2015)
141. B. Q. Lv, N. Xu, H. M. Weng, J. Z. Ma, P. Richard, X. C. Huang, L. X. Zhao, G. F. Chen, C. E. Matt, F. Bisti, V. N. Strocov, J. Mesot, Z. Fang, X. Dai, T. Qian, M. Shi, and H. Ding, Observation of Weyl nodes in TaAs, *Nat. Phys.* 11(9), 724 (2015)
142. J. Z. Ma, J. B. He, Y. F. Xu, B. Q. Lv, D. Chen, W. L. Zhu, S. Zhang, L. Y. Kong, X. Gao, L. Y. Rong, Y. B. Huang, P. Richard, C. Y. Xi, E. S. Choi, Y. Shao, Y. L. Wang, H. J. Gao, X. Dai, C. Fang, H. M. Weng, G. F. Chen, T. Qian, and H. Ding, Three-component fermions with surface Fermi arcs in tungsten carbide, *Nat. Phys.* 14(4), 349 (2018)
143. S. Y. Xu, N. Alidoust, I. Belopolski, Z. Yuan, G. Bian, T. R. Chang, H. Zheng, V. N. Strocov, D. S. Sanchez, G. Chang, C. Zhang, D. Mou, Y. Wu, L. Huang, C. C. Lee, S. M. Huang, B. K. Wang, A. Bansil, H. T. Jeng, T. Neupert, A. Kaminski, H. Lin, S. Jia, and M. Zahid Hasan, Discovery of a Weyl fermion state with Fermi arcs in niobium arsenide, *Nat. Phys.* 11(9), 748 (2015)
144. L. X. Yang, Z. K. Liu, Y. Sun, H. Peng, H. F. Yang, T. Zhang, B. Zhou, Y. Zhang, Y. F. Guo, M. Rahn, D. Prabhakaran, Z. Hussain, S. K. Mo, C. Felser, B. Yan, and Y. L. Chen, Weyl semimetal phase in the noncentrosymmetric compound TaAs, *Nat. Phys.* 11(9), 728 (2015)
145. Z. K. Liu, B. Zhou, Y. Zhang, Z. J. Wang, H. M. Weng, D. Prabhakaran, S. K. Mo, Z. X. Shen, Z. Fang, X. Dai, Z. Hussain, and Y. L. Chen, Discovery of a three-dimensional topological Dirac semimetal, Na_3Bi, *Science* 343(6173), 864 (2014)
146. Z. K. Liu, J. Jiang, B. Zhou, Z. J. Wang, Y. Zhang, H. M. Weng, D. Prabhakaran, S. K. Mo, H. Peng, P. Dudin, T. Kim, M. Hoesch, Z. Fang, X. Dai, Z. X. Shen, D. L. Feng, Z. Hussain, and Y. L. Chen, A stable three-dimensional topological Dirac semimetal Cd_3As_2, *Nat. Mater.* 13(7), 677 (2014)
147. M. Neupane, S. Y. Xu, R. Sankar, N. Alidoust, G. Bian, C. Liu, I. Belopolski, T. R. Chang, H. T. Jeng, H. Lin, A. Bansil, F. Chou, and M. Z. Hasan, Observation of a three-dimensional topological Dirac semimetal phase in high-mobility Cd_3As_2, *Nat. Commun.* 5(1), 3786 (2014)
148. G. Xu, H. Weng, Z. Wang, X. Dai, and Z. Fang, Chern semimetal and the quantized anomalous Hall

effect in $HgCr_2Se_4$, *Phys. Rev. Lett.* 107(18), 186806 (2011)

149. S. H. Do, K. Kaneko, R. Kajimoto, K. Kamazawa, M. B. Stone, J. Y. Y. Lin, S. Itoh, T. Masuda, G. D. Samolyuk, E. Dagotto, W. R. Meier, B. C. Sales, H. Miao, and A. D. Christianson, Damped Dirac magnon in the metallic Kagomé antiferromagnet FeSn, *Phys. Rev. B* 105(18), L180403 (2022)
150. Z. Lin, C. Wang, P. Wang, S. Yi, L. Li, Q. Zhang, Y. Wang, Z. Wang, H. Huang, Y. Sun, Y. Huang, D. Shen, D. Feng, Z. Sun, J. H. Cho, C. Zeng, and Z. Zhang, Dirac fermions in antiferromagnetic FeSn Kagomé lattices with combined space inversion and time-reversal symmetry, *Phys. Rev. B* 102(15), 155103 (2020)
151. M. Kang, L. Ye, S. Fang, J. S. You, A. Levitan, M. Han, J. I. Facio, C. Jozwiak, A. Bostwick, E. Rotenberg, M. K. Chan, R. D. McDonald, D. Graf, K. Kaznatcheev, E. Vescovo, D. C. Bell, E. Kaxiras, J. van den Brink, M. Richter, M. Prasad Ghimire, J. G. Checkelsky, and R. Comin, Dirac fermions and flat bands in the ideal Kagomé metal FeSn, *Nat. Mater.* 19(2), 163 (2020)
152. M. Han, H. Inoue, S. Fang, C. John, L. Ye, M. K. Chan, D. Graf, T. Suzuki, M. P. Ghimire, W. J. Cho, E. Kaxiras, and J. G. Checkelsky, Evidence of two-dimensional flat band at the surface of antiferromagnetic Kagomé metal FeSn, *Nat. Commun.* 12(1), 5345 (2021)
153. S. H. Lee, Y. Kim, B. Cho, J. Park, M. S. Kim, K. Park, H. Jeon, M. Jung, K. Park, J. D. Lee, and J. Seo, Spin-polarized and possible pseudospin-polarized scanning tunneling microscopy in Kagomé metal FeSn, *Commun. Phys.* 5(1), 235 (2022)
154. B. C. Sales, J. Yan, W. R. Meier, A. D. Christianson, S. Okamoto, and M. A. McGuire, Electronic, magnetic, and thermodynamic properties of the Kagomé layer compound FeSn, *Phys. Rev. Mater.* 3(11), 114203 (2019)
155. C. Liu, C. J. Yi, X. Y. Wang, J. L. Shen, T. Xie, L. Yang, T. Fennel, U. Stuhr, S. L. Li, H. M. Weng, Y. G. Shi, E. K. Liu, and H. Q. Luo, Anisotropic magnetoelastic response in the magnetic Weyl semimetal $Co_3Sn_2S_2$, *Sci. China Phys. Mech. Astron.* 64(5), 257511 (2021)
156. D. F. Liu, E. K. Liu, Q. N. Xu, J. L. Shen, Y. W. Li, D. Pei, A. J. Liang, P. Dudin, T. K. Kim, C. Cacho, Y. F. Xu, Y. Sun, L. X. Yang, Z. K. Liu, C. Felser, S. S. P. Parkin, and Y. L. Chen, Direct observation of the spin–orbit coupling effect in magnetic Weyl semimetal $Co_3Sn_2S_2$, *npj Quantum Mater.* 7, 11 (2022)
157. M. Kanagaraj, J. Ning, and L. He, Topological $Co_3Sn_2S_2$ magnetic Weyl semimetal: From fundamental understanding to diverse fields of study, *Reviews in Physics* 8, 100072 (2022)
158. I. Belopolski, T. A. Cochran, X. Liu, Z. J. Cheng, X. P. Yang, Z. Guguchia, S. S. Tsirkin, J. X. Yin, P. Vir, G. S. Thakur, S. S. Zhang, J. Zhang, K. Kaznatcheev, G. Cheng, G. Chang, D. Multer, N. Shumiya, M. Litskevich, E. Vescovo, T. K. Kim, C. Cacho, N. Yao, C. Felser, T. Neupert, and M. Z. Hasan, Signatures of Weyl fermion annihilation in a correlated Kagomé magnet, *Phys. Rev. Lett.* 127(25), 256403 (2021)
159. G. Li, Q. Xu, W. Shi, C. Fu, L. Jiao, M. E. Kamminga, M. Yu, H. Tüysüz, N. Kumar, V. Süß, R. Saha, A. K. Srivastava, S. Wirth, G. Auffermann, J. Gooth, S. Parkin, Y. Sun, E. Liu, and C. Felser, Surface states in bulk single crystal of topological semimetal $Co_3Sn_2S_2$ toward water oxidation, *Sci. Adv.* 5(8), eaaw9867 (2019)
160. Q. Xu, E. Liu, W. Shi, L. Muechler, J. Gayles, C. Felser, and Y. Sun, Topological surface Fermi arcs in the magnetic Weyl semimetal $Co_3Sn_2S_2$, *Phys. Rev. B* 97(23), 235416 (2018)
161. Q. Wang, Y. Xu, R. Lou, Z. Liu, M. Li, Y. Huang, D. Shen, H. Weng, S. Wang, and H. Lei, Large intrinsic anomalous Hall effect in half-metallic ferromagnet $Co_3Sn_2S_2$ with magnetic Weyl fermions, *Nat. Commun.* 9(1), 3681 (2018)
162. M. Tanaka, Y. Fujishiro, M. Mogi, Y. Kaneko, T. Yokosawa, N. Kanazawa, S. Minami, T. Koretsune, R. Arita, S. Tarucha, M. Yamamoto, and Y. Tokura, Topological Kagomé magnet $Co_3Sn_2S_2$ thin flakes with high electron mobility and large anomalous Hall effect, *Nano Lett.* 20(10), 7476 (2020)
163. H. Reichlova, T. Janda, J. Godinho, A. Markou, D. Kriegner, R. Schlitz, J. Zelezny, Z. Soban, M. Bejarano, H. Schultheiss, P. Nemec, T. Jungwirth, C. Felser, J. Wunderlich, and S. T. B. Goennenwein, Imaging and writing magnetic domains in the non-collinear antiferromagnet Mn_3Sn, *Nat. Commun.* 10(1), 5459 (2019)
164. T. Chen, T. Tomita, S. Minami, M. Fu, T. Koretsune, M. Kitatani, I. Muhammad, D. Nishio-Hamane, R. Ishii, F. Ishii, R. Arita, and S. Nakatsuji, Anomalous transport due to Weyl fermions in the chiral antiferromagnets Mn_3X, X = Sn, Ge, *Nat. Commun.* 12(1), 572 (2021)
165. J. R. Soh, F. de Juan, N. Qureshi, H. Jacobsen, H. Y. Wang, Y. F. Guo, and A. T. Boothroyd, Ground-state magnetic structure of Mn_3Ge, *Phys. Rev. B* 101(14), 140411 (2020)
166. J. Liu and L. Balents, Anomalous Hall effect and topological defects in antiferromagnetic Weyl semimetals: Mn_3Sn/Ge, *Phys. Rev. Lett.* 119(8), 087202 (2017)
167. H. Yang, Y. Sun, Y. Zhang, W. J. Shi, S. S. P. Parkin, and B. Yan, Topological Weyl semimetals in the chiral antiferromagnetic materials Mn_3Ge and Mn_3Sn, *New J. Phys.* 19(1), 015008 (2017)
168. N. Kiyohara, T. Tomita, and S. Nakatsuji, Giant anomalous Hall effect in the chiral antiferromagnet Mn_3Ge, *Phys. Rev. Appl.* 5(6), 064009 (2016)
169. T. Higo, D. Qu, Y. Li, C. L. Chien, Y. Otani, and S. Nakatsuji, Anomalous Hall effect in thin films of the Weyl antiferromagnet Mn_3Sn, *Appl. Phys. Lett.* 113(20), 202402 (2018)
170. T. Matsuda, N. Kanda, T. Higo, N. P. Armitage, S. Nakatsuji, and R. Matsunaga, Room-temperature terahertz anomalous Hall effect in Weyl antiferromagnet Mn_3Sn thin films, *Nat. Commun.* 11(1), 909 (2020)
171. J. M. Taylor, A. Markou, E. Lesne, P. K. Sivakumar, C. Luo, F. Radu, P. Werner, C. Felser, and S. S. P. Parkin, Anomalous and topological Hall effects in epitaxial thin films of the noncollinear antiferromagnet Mn_3Sn, *Phys. Rev. B* 101(9), 094404 (2020)
172. M. Ikhlas, T. Tomita, T. Koretsune, M. T. Suzuki, D.

Nishio-Hamane, R. Arita, Y. Otani, and S. Nakatsuji, Large anomalous Nernst effect at room temperature in a chiral antiferromagnet, *Nat. Phys.* 13(11), 1085 (2017)
173. C. Wuttke, F. Caglieris, S. Sykora, F. Scaravaggi, A. U. B. Wolter, K. Manna, V. Süss, C. Shekhar, C. Felser, B. Büchner, and C. Hess, Berry curvature unravelled by the anomalous Nernst effect in Mn_3Ge, *Phys. Rev. B* 100(8), 085111 (2019)
174. X. Li, C. Collignon, L. Xu, H. Zuo, A. Cavanna, U. Gennser, D. Mailly, B. Fauque, L. Balents, Z. Zhu, and K. Behnia, Chiral domain walls of Mn_3Sn and their memory, *Nat. Commun.* 10(1), 3021 (2019)
175. P. K. Rout, P. V. P. Madduri, S. K. Manna, and A. K. Nayak, Field-induced topological Hall effect in the noncoplanar triangular antiferromagnetic geometry of Mn_3Sn, *Phys. Rev. B* 99(9), 094430 (2019)
176. L. Xu, X. Li, L. Ding, K. Behnia, and Z. Zhu, Planar Hall effect caused by the memory of antiferromagnetic domain walls in Mn_3Ge, *Appl. Phys. Lett.* 117(22), 222403 (2020)
177. M. Kimata, H. Chen, K. Kondou, S. Sugimoto, P. K. Muduli, M. Ikhlas, Y. Omori, T. Tomita, A. H. MacDonald, S. Nakatsuji, and Y. Otani, Magnetic and magnetic inverse spin Hall effects in a non-collinear antiferromagnet, *Nature* 565(7741), 627 (2019)
178. P. Li, J. Koo, W. Ning, J. Li, L. Miao, L. Min, Y. Zhu, Y. Wang, N. Alem, C. X. Liu, Z. Mao, and B. Yan, Giant room temperature anomalous Hall effect and tunable topology in a ferromagnetic topological semimetal Co_2MnAl, *Nat. Commun.* 11(1), 3476 (2020)
179. G. Chang, S. Y. Xu, X. Zhou, S. M. Huang, B. Singh, B. Wang, I. Belopolski, J. Yin, S. Zhang, A. Bansil, H. Lin, and M. Z. Hasan, Topological Hopf and chain link semimetal states and their application to Co_2MnGa, *Phys. Rev. Lett.* 119(15), 156401 (2017)
180. I. Belopolski, G. Chang, T. A. Cochran, Z. J. Cheng, X. P. Yang, C. Hugelmeyer, K. Manna, J. X. Yin, G. Cheng, D. Multer, M. Litskevich, N. Shumiya, S. S. Zhang, C. Shekhar, N. B. M. Schroter, A. Chikina, C. Polley, B. Thiagarajan, M. Leandersson, J. Adell, S. M. Huang, N. Yao, V. N. Strocov, C. Felser, and M. Z. Hasan, Observation of a linked-loop quantum state in a topological magnet, *Nature* 604(7907), 647 (2022)
181. Z. Wang, M. G. Vergniory, S. Kushwaha, M. Hirschberger, E. V. Chulkov, A. Ernst, N. P. Ong, R. J. Cava, and B. A. Bernevig, Time-reversal-breaking Weyl fermions in magnetic Heusler alloys, *Phys. Rev. Lett.* 117(23), 236401 (2016)
182. G. Chang, S. Y. Xu, H. Zheng, B. Singh, C. H. Hsu, G. Bian, N. Alidoust, I. Belopolski, D. S. Sanchez, S. Zhang, H. Lin, and M. Z. Hasan, Room-temperature magnetic topological Weyl fermion and nodal line semimetal states in half-metallic Heusler Co_2TiX (X= Si, Ge, or Sn), *Sci. Rep.* 6(1), 38839 (2016)
183. R. Y. Umetsu, K. Kobayashi, A. Fujita, R. Kainuma, and K. Ishida, Magnetic properties and stability of L21 and B2 phases in the Co_2MnAl Heusler alloy, *J. Appl. Phys.* 103(7), 07D718 (2008)
184. A. W. Carbonari, R. N. Saxena, W. Jr Pendl, J. Mestnik Filho, R. N. Attili, M. Olzon-Dionysio, and S. D. de Souza, Magnetic hyperfine field in the Heusler alloys Co_2YZ (Y = V, Nb, Ta, Cr; Z = Al, Ga), *J. Magn. Magn. Mater.* 163(3), 313 (1996)
185. Z. Yan, R. Bi, H. Shen, L. Lu, S. C. Zhang, and Z. Wang, Nodal-link semimetals, *Phys. Rev. B* 96(4), 041103 (2017)
186. M. Ezawa, Topological semimetals carrying arbitrary Hopf numbers: Fermi surface topologies of a Hopf link, Solomon's knot, trefoil knot, and other linked nodal varieties, *Phys. Rev. B* 96(4), 041202 (2017)
187. P. Y. Chang and C. H. Yee, Weyl-link semimetals, *Phys. Rev. B* 96(8), 081114 (2017)
188. K. Sumida, Y. Sakuraba, K. Masuda, T. Kono, M. Kakoki, K. Goto, W. Zhou, K. Miyamoto, Y. Miura, T. Okuda, and A. Kimura, Spin-polarized Weyl cones and giant anomalous Nernst effect in ferromagnetic Heusler films, *Commun. Mater.* 1(1), 89 (2020)
189. Q. Wu, A. A. Soluyanov, and T. Bzdusek, Non-Abelian band topology in noninteracting metals, *Science* 365(6459), 1273 (2019)
190. I. Belopolski, K. Manna, D. S. Sanchez, G. Chang, B. Ernst, J. Yin, S. S. Zhang, T. Cochran, N. Shumiya, H. Zheng, B. Singh, G. Bian, D. Multer, M. Litskevich, X. Zhou, S. M. Huang, B. Wang, T. R. Chang, S. Y. Xu, A. Bansil, C. Felser, H. Lin, and M. Z. Hasan, Discovery of topological Weyl fermion lines and drumhead surface states in a room temperature magnet, *Science* 365(6459), 1278 (2019)
191. C. Zhong, Y. Chen, Z. M. Yu, Y. Xie, H. Wang, S. A. Yang, and S. Zhang, Three-dimensional pentagon carbon with a genesis of emergent fermions, *Nat. Commun.* 8(1), 15641 (2017)
192. A. Bouhon, Q. S. Wu, R. J. Slager, H. Weng, O. V. Yazyev, and T. Bzdušek, Non-Abelian reciprocal braiding of Weyl points and its manifestation in ZrTe, *Nat. Phys.* 16(11), 1137 (2020)
193. J. Yuan, X. Shi, H. Su, X. Zhang, X. Wang, N. Yu, Z. Zou, W. Zhao, J. Liu, and Y. Guo, Magnetization tunable Weyl states in EuB_6, *Phys. Rev. B* 106(5), 054411 (2022)
194. S. Y. Gao, S. Xu, H. Li, C. J. Yi, S. M. Nie, Z. C. Rao, H. Wang, Q. X. Hu, X. Z. Chen, W. H. Fan, J. R. Huang, Y. B. Huang, N. Pryds, M. Shi, Z. J. Wang, Y. G. Shi, T. L. Xia, T. Qian, and H. Ding, Time-reversal symmetry breaking driven topological phase transition in EuB_6, *Phys. Rev. X* 11(2), 021016 (2021)
195. S. Nie, Y. Sun, F. B. Prinz, Z. Wang, H. Weng, Z. Fang, and X. Dai, Magnetic semimetals and quantized anomalous Hall effect in EuB_6, *Phys. Rev. Lett.* 124(7), 076403 (2020)
196. X. Zhang, S. von Molnar, Z. Fisk, and P. Xiong, Spin-dependent electronic states of the ferromagnetic semimetal EuB_6, *Phys. Rev. Lett.* 100(16), 167001 (2008)
197. J. Kim, W. Ku, C. C. Lee, D. S. Ellis, B. K. Cho, A. H. Said, Y. Shvyd'ko, and Y. J. Kim, Spin-split conduction band in EuB_6 and tuning of half-metallicity with external stimuli, *Phys. Rev. B* 87(15), 155104 (2013)
198. S. Süllow, I. Prasad, M. C. Aronson, J. L. Sarrao, Z. Fisk, D. Hristova, A. H. Lacerda, M. F. Hundley, A. Vigliante, and D. Gibbs, Structure and magnetic order

of EuB_6, *Phys. Rev. B* 57(10), 5860 (1998)
199. M. L. Brooks, T. Lancaster, S. J. Blundell, W. Hayes, F. L. Pratt, and Z. Fisk, Magnetic phase separation in EuB_6 detected by muon spin rotation, *Phys. Rev. B* 70(2), 020401 (2004)
200. L. Degiorgi, E. Felder, H. R. Ott, J. L. Sarrao, and Z. Fisk, Low-temperature anomalies and ferromagnetism of EuB_6, *Phys. Rev. Lett.* 79(25), 5134 (1997)
201. C. N. Guy, S. von Molnar, J. Etourneau, and Z. Fisk, Charge transport and pressure dependence of T_c of single crystal, ferromagnetic EuB_6, *Solid State Commun.* 33(10), 1055 (1980)
202. P. Nyhus, S. Yoon, M. Kauffman, S. L. Cooper, Z. Fisk, and J. Sarrao, Spectroscopic study of bound magnetic polaron formation and the metal-semiconductor transition in EuB_6, *Phys. Rev. B* 56(5), 2717 (1997)
203. G. Beaudin, L. M. Fournier, A. D. Bianchi, M. Nicklas, M. Kenzelmann, M. Laver, and W. Witczak-Krempa, Possible quantum nematic phase in a colossal magnetoresistance material, *Phys. Rev. B* 105(3), 035104 (2022)
204. W. L. Liu, X. Zhang, S. M. Nie, Z. T. Liu, X. Y. Sun, H. Y. Wang, J. Y. Ding, Q. Jiang, L. Sun, F. H. Xue, Z. Huang, H. Su, Y. C. Yang, Z. C. Jiang, X. L. Lu, J. Yuan, S. Cho, J. S. Liu, Z. H. Liu, M. Ye, S. L. Zhang, H. M. Weng, Z. Liu, Y. F. Guo, Z. J. Wang, and D. W. Shen, Spontaneous ferromagnetism induced topological transition in EuB_6, *Phys. Rev. Lett.* 129(16), 166402 (2022)
205. Q. Zeng, C. Yi, J. Shen, B. Wang, H. Wei, Y. Shi, and E. Liu, Berry curvature induced antisymmetric in-plane magneto-transport in magnetic Weyl EuB_6, *Appl. Phys. Lett.* 121(16), 162405 (2022)
206. B. Chen, J. H. Yang, H. D. Wang, M. Imai, H. Ohta, C. Michioka, K. Yoshimura, and M. H. Fang, Magnetic properties of layered itinerant electron ferromagnet Fe_3GeTe_2, *J. Phys. Soc. Jpn.* 82(12), 124711 (2013)
207. Y. Zhang, H. Lu, X. Zhu, S. Tan, W. Feng, Q. Liu, W. Zhang, Q. Chen, Y. Liu, X. Luo, D. Xie, L. Luo, Z. Zhang, and X. Lai, Emergence of Kondo lattice behavior in a van der Waals itinerant ferromagnet, Fe_3GeTe_2, *Sci. Adv.* 4(1), eaao6791 (2018)
208. Y. Deng, Y. Yu, Y. Song, J. Zhang, N. Z. Wang, Z. Sun, Y. Yi, Y. Z. Wu, S. Wu, J. Zhu, J. Wang, X. H. Chen, and Y. Zhang, Gate-tunable room-temperature ferromagnetism in two-dimensional Fe_3GeTe_2, *Nature* 563(7729), 94 (2018)
209. X. Lin and J. Ni, Layer-dependent intrinsic anomalous Hall effect in Fe_3GeTe_2, *Phys. Rev. B* 100(8), 085403 (2019)
210. K. Kim, J. Seo, E. Lee, K. T. Ko, B. S. Kim, B. G. Jang, J. M. Ok, J. Lee, Y. J. Jo, W. Kang, J. H. Shim, C. Kim, H. W. Yeom, B. Il Min, B. J. Yang, and J. S. Kim, Large anomalous Hall current induced by topological nodal lines in a ferromagnetic van der Waals semimetal, *Nat. Mater.* 17(9), 794 (2018)
211. H. J. Deiseroth, K. Aleksandrov, C. Reiner, L. Kienle, and R. K. Kremer, Fe_3GeTe_2 and Ni_3GeTe_2 – two new layered transition-metal compounds: Crystal structures, HRTEM investigations, and magnetic and electrical properties, *Eur. J. Inorg. Chem.* 2006(8), 1561 (2006)
212. J. Yi, H. Zhuang, Q. Zou, Z. Wu, G. Cao, S. Tang, S. A. Calder, P. R. C. Kent, D. Mandrus, and Z. Gai, Competing antiferromagnetism in a quasi-2D itinerant ferromagnet: Fe_3GeTe_2, *2D Mater.* 4, 011005 (2016)
213. Y. Wang, C. Xian, J. Wang, B. Liu, L. Ling, L. Zhang, L. Cao, Z. Qu, and Y. Xiong, Anisotropic anomalous Hall effect in triangular itinerant ferromagnet Fe_3GeTe_2, *Phys. Rev. B* 96(13), 134428 (2017)
214. J. Ke, M. Yang, W. Xia, H. Zhu, C. Liu, R. Chen, C. Dong, W. Liu, M. Shi, Y. Guo, and J. Wang, Magnetic and magneto-transport studies of two-dimensional ferromagnetic compound Fe_3GeTe_2, *J. Phys.: Condens. Matter* 32(40), 405805 (2020)
215. H. Feng, Y. Li, Y. Shi, H. Y. Xie, Y. Li, and Y. Xu, Resistance anomaly and linear magnetoresistance in thin flakes of itinerant ferromagnet Fe_3GeTe_2, *Chin. Phys. Lett.* 39(7), 077501 (2022)
216. J. Xu, W. A. Phelan, and C. L. Chien, Large anomalous Nernst effect in a van der Waals ferromagnet Fe_3GeTe_2, *Nano Lett.* 19(11), 8250 (2019)
217. Z. Fei, B. Huang, P. Malinowski, W. Wang, T. Song, J. Sanchez, W. Yao, D. Xiao, X. Zhu, A. F. May, W. Wu, D. H. Cobden, J. H. Chu, and X. Xu, Two-dimensional itinerant ferromagnetism in atomically thin Fe_3GeTe_2, *Nat. Mater.* 17(9), 778 (2018)
218. Q. Li, M. Yang, C. Gong, R. V. Chopdekar, A. T. N' Diaye, J. Turner, G. Chen, A. Scholl, P. Shafer, E. Arenholz, A. K. Schmid, S. Wang, K. Liu, N. Gao, A. S. Admasu, S. W. Cheong, C. Hwang, J. Li, F. Wang, X. Zhang, and Z. Qiu, Patterning-induced ferromagnetism of Fe_3GeTe_2 van der Waals materials beyond room temperature, *Nano Lett.* 18(9), 5974 (2018)
219. C. Tan, J. Lee, S. G. Jung, T. Park, S. Albarakati, J. Partridge, M. R. Field, D. G. McCulloch, L. Wang, and C. Lee, Hard magnetic properties in nanoflake van der Waals Fe_3GeTe_2, *Nat. Commun.* 9(1), 1554 (2018)
220. X. Wang, J. Tang, X. Xia, C. He, J. Zhang, Y. Liu, C. Wan, C. Fang, C. Guo, W. Yang, Y. Guang, X. Zhang, H. Xu, J. Wei, M. Liao, X. Lu, J. Feng, X. Li, Y. Peng, H. Wei, R. Yang, D. Shi, X. Zhang, Z. Han, Z. Zhang, G. Zhang, G. Yu, and X. Han, Current-driven magnetization switching in a van der Waals ferromagnet Fe_3GeTe_2, *Sci. Adv.* 5(8), eaaw8904 (2019)
221. S. Y. Park, D. S. Kim, Y. Liu, J. Hwang, Y. Kim, W. Kim, J. Y. Kim, C. Petrovic, C. Hwang, S. K. Mo, H. J. Kim, B. C. Min, H. C. Koo, J. Chang, C. Jang, J. W. Choi, and H. Ryu, Controlling the magnetic anisotropy of the van der Waals ferromagnet Fe_3GeTe_2 through hole doping, *Nano Lett.* 20(1), 95 (2020)
222. H. Wang, Y. Liu, P. Wu, W. Hou, Y. Jiang, X. Li, C. Pandey, D. Chen, Q. Yang, H. Wang, D. Wei, N. Lei, W. Kang, L. Wen, T. Nie, W. Zhao, and K. L. Wang, Above room-temperature ferromagnetism in wafer-scale two-dimensional van der Waals Fe_3GeTe_2 tailored by a topological insulator, *ACS Nano* 14(8), 10045 (2020)
223. I. K. Park, C. Gong, K. Kim, and G. Lee, Controlling interlayer magnetic coupling in the two-dimensional magnet Fe_3GeTe_2, *Phys. Rev. B* 105(1), 014406 (2022)
224. H. P. Wang, D. S. Wu, Y. G. Shi, and N. L. Wang,

Anisotropic transport and optical spectroscopy study on antiferromagnetic triangular lattice $EuCd_2As_2$: An interplay between magnetism and charge transport properties, *Phys. Rev. B* 94(4), 045112 (2016)

225. M. C. Rahn, J. R. Soh, S. Francoual, L. S. I. Veiga, J. Strempfer, J. Mardegan, D. Y. Yan, Y. F. Guo, Y. G. Shi, and A. T. Boothroyd, Coupling of magnetic order and charge transport in the candidate Dirac semimetal $EuCd_2As_2$, *Phys. Rev. B* 97(21), 214422 (2018)
226. K. M. Taddei, L. Yin, L. D. Sanjeewa, Y. Li, J. Xing, C. dela Cruz, D. Phelan, A. S. Sefat, and D. S. Parker, Single pair of Weyl nodes in the spin-canted structure of $EuCd_2As_2$, *Phys. Rev. B* 105(14), L140401 (2022)
227. J. Ma, H. Wang, S. Nie, C. Yi, Y. Xu, H. Li, J. Jandke, W. Wulfhekel, Y. Huang, D. West, P. Richard, A. Chikina, V. N. Strocov, J. Mesot, H. Weng, S. Zhang, Y. Shi, T. Qian, M. Shi, and H. Ding, Emergence of nontrivial low-energy Dirac fermions in antiferromagnetic $EuCd_2As_2$, *Adv. Mater.* 32(14), 1907565 (2020)
228. X. Cao, J. X. Yu, P. Leng, C. Yi, X. Chen, Y. Yang, S. Liu, L. Kong, Z. Li, X. Dong, Y. Shi, M. Bibes, R. Peng, J. Zang, and F. Xiu, Giant nonlinear anomalous Hall effect induced by spin-dependent band structure evolution, *Phys. Rev. Res.* 4(2), 023100 (2022)
229. I. Schellenberg, U. Pfannenschmidt, M. Eul, C. Schwickert, and R. Pöttgen, A ^{121}Sb and ^{151}Eu Mössbauer spectroscopic investigation of $EuCd_2X_2$ (X = P, As, Sb) and $YbCd_2Sb_2$, *Z. Anorg. Allg. Chem.* 637(12), 1863 (2011)
230. L. L. Wang, N. H. Jo, B. Kuthanazhi, Y. Wu, R. J. McQueeney, A. Kaminski, and P. C. Canfield, Single pair of Weyl fermions in the half-metallic semimetal $EuCd_2As_2$, *Phys. Rev. B* 99(24), 245147 (2019)
231. J. R. Soh, C. Donnerer, K. M. Hughes, E. Schierle, E. Weschke, D. Prabhakaran, and A. T. Boothroyd, Magnetic and electronic structure of the layered rare-earth pnictide $EuCd_2Sb_2$, *Phys. Rev. B* 98(6), 064419 (2018)
232. J. Krishna, T. Nautiyal, and T. Maitra, First-principles study of electronic structure, transport, and optical properties of $EuCd_2As_2$, *Phys. Rev. B* 98(12), 125110 (2018)
233. Y. Sun, Y. Li, S. Li, C. Yi, H. Deng, X. Du, L. Liu, C. Zhu, Y. Li, Z. Wang, H. Mao, Y. Shi, and R. Wu, Experimental evidence for field-induced metamagnetic transition of $EuCd_2As_2$, *J. Rare Earths* 40(10), 1606 (2022)
234. G. Hua, S. Nie, Z. Song, R. Yu, G. Xu, and K. Yao, Dirac semimetal in type-IV magnetic space groups, *Phys. Rev. B* 98(20), 201116 (2018)
235. F. Schindler, A. M. Cook, M. G. Vergniory, Z. Wang, S. S. P. Parkin, B. A. Bernevig, and T. Neupert, Higher-order topological insulators, *Sci. Adv.* 4(6), eaat0346 (2018)
236. J. R. Soh, F. de Juan, M. G. Vergniory, N. B. M. Schröter, M. C. Rahn, D. Y. Yan, J. Jiang, M. Bristow, P. A. Reiss, J. N. Blandy, Y. F. Guo, Y. G. Shi, T. K. Kim, A. McCollam, S. H. Simon, Y. Chen, A. I. Coldea, and A. T. Boothroyd, Ideal Weyl semimetal induced by magnetic exchange, *Phys. Rev. B* 100(20), 201102 (2019)
237. L. A. Fenner, A. A. Dee, and A. S. Wills, Non-collinearity and spin frustration in the itinerant Kagomé ferromagnet Fe_3Sn_2, *J. Phys.: Condens. Matter* 21(45), 452202 (2009)
238. L. Ye, M. Kang, J. Liu, F. von Cube, C. R. Wicker, T. Suzuki, C. Jozwiak, A. Bostwick, E. Rotenberg, D. C. Bell, L. Fu, R. Comin, and J. G. Checkelsky, Massive Dirac fermions in a ferromagnetic Kagomé metal, *Nature* 555(7698), 638 (2018)
239. B. Malaman, B. Roques, A. Courtois, and J. Protas, Structure cristalline du stannure de fer Fe_3Sn_2, *Acta Crystallogr. B* 32(5), 1348 (1976)
240. G. L. Caer, B. Malaman, and B. Roques, Mossbauer effect study of Fe_3Sn_2, *J. Phys. F Met. Phys.* 8(2), 323 (1978)
241. B. Malaman, D. Fruchart, and G. L. Caer, Magnetic properties of Fe_3Sn_2 (II): Neutron diffraction study (and Mossbauer effect), *J. Phys. F Met. Phys.* 8(11), 2389 (1978)
242. G. Le Caer, B. Malaman, L. Haggstrom, and T. Ericsson, Magnetic properties of Fe_3Sn_2 (III): A ^{119}Sn Mossbauer study, *J. Phys. F Met. Phys.* 9(9), 1905 (1979)
243. Z. Lin, J. H. Choi, Q. Zhang, W. Qin, S. Yi, P. Wang, L. Li, Y. Wang, H. Zhang, Z. Sun, L. Wei, S. Zhang, T. Guo, Q. Lu, J. H. Cho, C. Zeng, and Z. Zhang, Flatbands and emergent ferromagnetic ordering in Fe_3Sn_2 Kagomé lattices, *Phys. Rev. Lett.* 121(9), 096401 (2018)
244. J. X. Yin, S. S. Zhang, H. Li, K. Jiang, G. Chang, B. Zhang, B. Lian, C. Xiang, I. Belopolski, H. Zheng, T. A. Cochran, S. Y. Xu, G. Bian, K. Liu, T. R. Chang, H. Lin, Z. Y. Lu, Z. Wang, S. Jia, W. Wang, and M. Z. Hasan, Giant and anisotropic many-body spin–orbit tunability in a strongly correlated Kagomé magnet, *Nature* 562(7725), 91 (2018)
245. Q. Wang, S. Sun, X. Zhang, F. Pang, and H. Lei, Anomalous Hall effect in a ferromagnetic Fe_3Sn_2 single crystal with a geometrically frustrated Fe bilayer Kagomé lattice, *Phys. Rev. B* 94(7), 075135 (2016)
246. Z. P. Hou, B. Ding, H. Li, G. Z. Xu, W. H. Wang, and G. H. Wu, Observation of new-type magnetic skymrions with extremerely high temperature stability and fabrication of skyrmion-based race-track memory device, *Acta Phys. Sin.* 67(13), 137509 (2018)
247. H. Li, B. Ding, J. Chen, Z. Li, Z. Hou, E. Liu, H. Zhang, X. Xi, G. Wu, and W. Wang, Large topological Hall effect in a geometrically frustrated Kagomé magnet Fe_3Sn_2, *Appl. Phys. Lett.* 114(19), 192408 (2019)
248. C. D. O'Neill, A. S. Wills, and A. D. Huxley, Possible topological contribution to the anomalous Hall effect of the noncollinear ferromagnet Fe_3Sn_2, *Phys. Rev. B* 100(17), 174420 (2019)
249. Q. Wang, Q. Yin, and H. Lei, Giant topological Hall effect of ferromagnetic Kagomé metal Fe_3Sn_2, *Chin. Phys. B* 29(1), 017101 (2020)
250. Z. Hou, W. Ren, B. Ding, G. Xu, Y. Wang, B. Yang, Q. Zhang, Y. Zhang, E. Liu, F. Xu, W. Wang, G. Wu, X. Zhang, B. Shen, and Z. Zhang, Observation of various and spontaneous magnetic skyrmionic bubbles at room temperature in a frustrated Kagomé magnet with

uniaxial magnetic anisotropy, *Adv. Mater.* 29(29), 1701144 (2017)

251. Z. Hou, Q. Zhang, G. Xu, C. Gong, B. Ding, Y. Wang, H. Li, E. Liu, F. Xu, H. Zhang, Y. Yao, G. Wu, X. X. Zhang, and W. Wang, Creation of single chain of nanoscale skyrmion bubbles with record-high temperature stability in a geometrically confined nanostripe, *Nano Lett.* 18(2), 1274 (2018)
252. L. Gao, S. Shen, Q. Wang, W. Shi, Y. Zhao, C. Li, W. Cao, C. Pei, J. Y. Ge, G. Li, J. Li, Y. Chen, S. Yan, and Y. Qi, Anomalous Hall effect in ferrimagnetic metal RMn_6Sn_6 (R = Tb, Dy, Ho) with clean Mn Kagomé lattice, *Appl. Phys. Lett.* 119(9), 092405 (2021)
253. J. X. Yin, W. Ma, T. A. Cochran, X. Xu, S. S. Zhang, H. J. Tien, N. Shumiya, G. Cheng, K. Jiang, B. Lian, Z. Song, G. Chang, I. Belopolski, D. Multer, M. Litskevich, Z. J. Cheng, X. P. Yang, B. Swidler, H. Zhou, H. Lin, T. Neupert, Z. Wang, N. Yao, T. R. Chang, S. Jia, and M. Zahid Hasan, Quantum-limit Chern topological magnetism in $TbMn_6Sn_6$, *Nature* 583(7817), 533 (2020)
254. D. Chen, C. Le, C. Fu, H. Lin, W. Schnelle, Y. Sun, and C. Felser, Large anomalous Hall effect in the Kagomé ferromagnet $LiMn_6Sn_6$, *Phys. Rev. B* 103(14), 144410 (2021)
255. B. C. El Idrissi, G. Venturini, and B. Malaman, Crystal structures of RFe_6Sn_6 (R = Sc, Y, Gd–Tm, Lu) rare-earth iron stannides, *Mater. Res. Bull.* 26(12), 1331 (1991)
256. G. Venturini, B. C. E. Idrissi, and B. Malaman, Magnetic properties of RMn_6Sn_6 (R = Sc, Y, Gd–Tm, Lu) compounds with $HfFe_6Ge_6$ type structure, *J. Magn. Magn. Mater.* 94(1–2), 35 (1991)
257. N. J. Ghimire, R. L. Dally, L. Poudel, D. C. Jones, D. Michel, N. T. Magar, M. Bleuel, M. A. McGuire, J. S. Jiang, J. F. Mitchell, J. W. Lynn, and I. I. Mazin, Competing magnetic phases and fluctuation-driven scalar spin chirality in the Kagomé metal YMn_6Sn_6, *Sci. Adv.* 6(51), eabe2680 (2020)
258. W. Ma, X. Xu, J. X. Yin, H. Yang, H. Zhou, Z. J. Cheng, Y. Huang, Z. Qu, F. Wang, M. Z. Hasan, and S. Jia, Rare earth engineering in RMn_6Sn_6 (R = Gd–Tm, Lu) topological Kagomé magnets, *Phys. Rev. Lett.* 126(24), 246602 (2021)
259. M. Li, Q. Wang, G. Wang, Z. Yuan, W. Song, R. Lou, Z. Liu, Y. Huang, Z. Liu, H. Lei, Z. Yin, and S. Wang, Dirac cone, flat band and saddle point in Kagomé magnet YMn_6Sn_6, *Nat. Commun.* 12(1), 3129 (2021)
260. X. Gu, C. Chen, W. S. Wei, L. L. Gao, J. Y. Liu, X. Du, D. Pei, J. S. Zhou, R. Z. Xu, Z. X. Yin, W. X. Zhao, Y. D. Li, C. Jozwiak, A. Bostwick, E. Rotenberg, D. Backes, L. S. I. Veiga, S. Dhesi, T. Hesjedal, G. van der Laan, H. F. Du, W. J. Jiang, Y. P. Qi, G. Li, W. J. Shi, Z. K. Liu, Y. L. Chen, and L. X. Yang, Robust Kagomé electronic structure in the topological quantum magnets XMn_6Sn_6 (X=Dy, Tb, Gd, Y), *Phys. Rev. B* 105(15), 155108 (2022)
261. S. Roychowdhury, A. M. Ochs, S. N. Guin, K. Samanta, J. Noky, C. Shekhar, M. G. Vergniory, J. E. Goldberger, and C. Felser, Large room temperature anomalous transverse thermoelectric effect in Kagomé antiferromagnet YMn_6Sn_6, *Adv. Mater.* 34(40), e2201350 (2022)
262. G. Dhakal, F. Cheenicode Kabeer, A. K. Pathak, F. Kabir, N. Poudel, R. Filippone, J. Casey, A. Pradhan Sakhya, S. Regmi, C. Sims, K. Dimitri, P. Manfrinetti, K. Gofryk, P. M. Oppeneer, and M. Neupane, Anisotropically large anomalous and topological Hall effect in a Kagomé magnet, *Phys. Rev. B* 104(16), L161115 (2021)
263. Q. Wang, K. J. Neubauer, C. Duan, Q. Yin, S. Fujitsu, H. Hosono, F. Ye, R. Zhang, S. Chi, K. Krycka, H. Lei, and P. Dai, Field-induced topological Hall effect and double-fan spin structure with a *c*-axis component in the metallic Kagomé antiferromagnetic compound YMn_6Sn_6, *Phys. Rev. B* 103, 014416 (2021)
264. F. Kabir, R. Filippone, G. Dhakal, Y. Lee, N. Poudel, J. Casey, A. P. Sakhya, S. Regmi, R. Smith, P. Manfrinetti, L. Ke, K. Gofryk, M. Neupane, and A. K. Pathak, Unusual magnetic and transport properties in $HoMn_6Sn_6$ Kagomé magnet, *Phys. Rev. Mater.* 6(6), 064404 (2022)
265. J. Lee and E. Mun, 0, Anisotropic magnetic property of single crystals RV_6Sn_6 (R=Y, Gd–Tm, Lu), *Phys. Rev. Mater.* 6(8), 083401 (2022)
266. S. Peng, Y. Han, G. Pokharel, J. Shen, Z. Li, M. Hashimoto, D. Lu, B. R. Ortiz, Y. Luo, H. Li, M. Guo, B. Wang, S. Cui, Z. Sun, Z. Qiao, S. D. Wilson, and J. He, Realizing Kagomé band structure in two-dimensional Kagomé surface states of RV_6Sn_6 (R=Gd, Ho), *Phys. Rev. Lett.* 127(26), 266401 (2021)
267. Y. Hu, X. Wu, Y. Yang, S. Gao, N. C. Plumb, A. P. Schnyder, W. Xie, J. Ma, and M. Shi, Tunable topological Dirac surface states and van Hove singularities in Kagomé metal GdV_6Sn_6, *Sci. Adv.* 8, eadd2024 (2022)
268. E. Cheng, W. Xia, X. Shi, H. Fang, C. Wang, C. Xi, S. Xu, D. C. Peets, L. Wang, H. Su, L. Pi, W. Ren, X. Wang, N. Yu, Y. Chen, W. Zhao, Z. Liu, Y. Guo, and S. Li, Magnetism-induced topological transition in $EuAs_3$, *Nat. Commun.* 12(1), 6970 (2021)
269. W. Bauhofer, M. Wittmann, and H. G. v Schnering, Structure, electrical and magnetic properties of $CaAs_3$, $SrAs_3$, $BaAs_3$ and $EuAs_3$, *J. Phys. Chem. Solids* 42(8), 687 (1981)
270. T. Chattopadhyay, H. G. v. Schnering, and P. J. Brown, Neutron diffraction study of the magnetic ordering in $EuAs_3$, *J. Magn. Magn. Mater.* 28(3), 247 (1982)
271. T. Chattopadhyay and P. J. Brown, Field-induced transverse-sine-wave-to-longitudinal-sine-wave transition in $EuAs_3$, *Phys. Rev. B* 38(1), 795 (1988)
272. T. Chatterji, K. D. Liß, T. Tschentscher, B. Janossy, J. Strempfer, and T. Brückel, High-energy non-resonant X-ray magnetic scattering from $EuAs_3$, *Solid State Commun.* 131(11), 713 (2004)
273. T. Chatterji and W. Henggeler, μSR investigation of the magnetic ordering in $EuAs_3$, *Solid State Commun.* 132(9), 617 (2004)
274. W. Bauhofer and K. A. McEwen, Anisotropic magnetoresistance of the semimetallic antiferromagnet $EuAs_3$, *Phys. Rev. B* 43(16), 13450 (1991)
275. L. Elcoro, B. J. Wieder, Z. Song, Y. Xu, B. Bradlyn, and B. A. Bernevig, Magnetic topological quantum

chemistry, *Nat. Commun.* 12(1), 5965 (2021)
276. Y. Xu, L. Elcoro, Z. D. Song, B. J. Wieder, M. G. Vergniory, N. Regnault, Y. Chen, C. Felser, and B. A. Bernevig, High-throughput calculations of magnetic topological materials, *Nature* 586(7831), 702 (2020)
277. W. Haruki, P. H. Chun, and V. Ashvin, Structure and topology of band structures in the 1651 magnetic space groups, *Sci. Adv.* 4, eaat8685 (2018)
278. J. Gao, Z. Guo, H. Weng, and Z. Wang, Magnetic band representations, Fu–Kane-like symmetry indicators, and magnetic topological materials, *Phys. Rev. B* 106(3), 035150 (2022)
279. K. Choudhary, K. F. Garrity, N. J. Ghimire, N. Anand, and F. Tavazza, High-throughput search for magnetic topological materials using spin–orbit spillage, machine learning, and experiments, *Phys. Rev. B* 103(15), 155131 (2021)
280. A. Bouhon, G. F. Lange, and R. J. Slager, Topological correspondence between magnetic space group representations and subdimensions, *Phys. Rev. B* 103(24), 245127 (2021)
281. J. Gooth, B. Bradlyn, S. Honnali, C. Schindler, N. Kumar, J. Noky, Y. Qi, C. Shekhar, Y. Sun, Z. Wang, B. A. Bernevig, and C. Felser, Axionic charge-density wave in the Weyl semimetal $(TaSe_4)_2I$, *Nature* 575(7782), 315 (2019)
282. L. Šmejkal, A. H. MacDonald, J. Sinova, S. Nakatsuji, and T. Jungwirth, Anomalous Hall antiferromagnets, *Nat. Rev. Mater.* 7(6), 482 (2022)
283. L. Šmejkal, J. Sinova, and T. Jungwirth, Emerging research landscape of altermagnetism, *Phys. Rev. X* 12(4), 040501 (2022)
284. L. Šmejkal, J. Sinova, and T. Jungwirth, Beyond conventional ferromagnetism and antiferromagnetism: A phase with nonrelativistic spin and crystal rotation symmetry, *Phys. Rev. X* 12(3), 031042 (2022)
285. N. J. Ghimire, A. S. Botana, J. S. Jiang, J. Zhang, Y. S. Chen, and J. F. Mitchell, Large anomalous Hall effect in the chiral-lattice antiferromagnet $CoNb_3S_6$, *Nat. Commun.* 9(1), 3280 (2018)
286. L. Šmejkal, A. B. Hellenes, R. González-Hernández, J. Sinova, and T. Jungwirth, Giant and tunneling magnetoresistance in unconventional collinear antiferromagnets with nonrelativistic spin–momentum coupling, *Phys. Rev. X* 12(1), 011028 (2022)
287. Z. Feng, X. Zhou, L. Šmejkal, L. Wu, Z. Zhu, H. Guo, R. González-Hernández, X. Wang, H. Yan, P. Qin, X. Zhang, H. Wu, H. Chen, Z. Meng, L. Liu, Z. Xia, J. Sinova, T. Jungwirth, and Z. Liu, An anomalous Hall effect in altermagnetic ruthenium dioxide, *Nat. Electron.* 5(11), 735 (2022)
288. B. Schrunk, Y. Kushnirenko, B. Kuthanazhi, J. Ahn, L. L. Wang, E. O'Leary, K. Lee, A. Eaton, A. Fedorov, R. Lou, V. Voroshnin, O. J. Clark, J. Sanchez-Barriga, S. L. Bud'ko, R. J. Slager, P. C. Canfield, and A. Kaminski, Emergence of Fermi arcs due to magnetic splitting in an antiferromagnet, *Nature* 603(7902), 610 (2022)
289. S. Karube, T. Tanaka, D. Sugawara, N. Kadoguchi, M. Kohda, and J. Nitta, Observation of spin-splitter torque in collinear antiferromagnetic RuO_2, *Phys. Rev. Lett.* 129(13), 137201 (2022)
290. H. Bai, L. Han, X. Y. Feng, Y. J. Zhou, R. X. Su, Q. Wang, L. Y. Liao, W. X. Zhu, X. Z. Chen, F. Pan, X. L. Fan, and C. Song, Observation of spin splitting torque in a collinear antiferromagnet RuO_2, *Phys. Rev. Lett.* 128(19), 197202 (2022)
291. D. F. Shao, S. H. Zhang, M. Li, C. B. Eom, and E. Y. Tsymbal, Spin-neutral currents for spintronics, *Nat. Commun.* 12(1), 7061 (2021)
292. R. González-Hernández, L. Smejkal, K. Vyborny, Y. Yahagi, J. Sinova, T. Jungwirth, and J. Zelezny, Efficient electrical spin splitter based on nonrelativistic collinear antiferromagnetism, *Phys. Rev. Lett.* 126(12), 127701 (2021)